

1 **Running head:** Photoperiod signaling via GRXS17

2

3 Corresponding author: Pascal Rey

4 CEA, DSV, IBEB, Laboratoire d'Ecophysiologie Moléculaire des Plantes, Saint-Paul-lez-

5 Durance, F-13108, France

6 Phone: ++33 442254776

7 E-mail: pascal.rey@cea.fr

8

9 **Research area:** Signaling and Response

10 **Secondary research area:** Genes, Development and Evolution

11

12

13

14

15

16

17

18

19

20

21

22

23

24

25 **Arabidopsis glutaredoxin S17 and its partner NF-YC11/NC2 $\alpha$  contribute**  
26 **to maintenance of the shoot apical meristem under long-day photoperiod**

27 Johannes Knuesting<sup>1,†</sup>, Christophe Riondet<sup>2,3,†</sup>, Carlos Maria<sup>4</sup>, Inga Kruse<sup>5</sup>, Noëlle  
28 Bécuwe<sup>6,7,8</sup>, Nicolas König<sup>1</sup>, Carsten Berndt<sup>9,10</sup>, Sébastien Tourrette<sup>6,7,8</sup>, Jocelyne  
29 Guillemot-Montoya<sup>2,3</sup>, Enrique Herrero<sup>4</sup>, Frédéric Gaymard<sup>11</sup>, Janneke Balk<sup>5</sup>, Gemma  
30 Belli<sup>4</sup>, Renate Scheibe<sup>1</sup>, Jean-Philippe Reichheld<sup>2,3</sup>, Nicolas Rouhier<sup>12,13</sup> and Pascal Rey<sup>6,7,8\*</sup>

31 <sup>1</sup>Department of Plant Physiology, FB5, University of Osnabrück, D-49069 Osnabrück,  
32 Germany

33 <sup>2</sup>Laboratoire Génome et Développement des Plantes, Université Perpignan Via Domitia, F-  
34 66860 Perpignan, France

35 <sup>3</sup>Laboratoire Génome et Développement des Plantes, CNRS, F-66860 Perpignan, France

36 <sup>4</sup>Departament de Ciències Mèdiques Bàsiques, IRBLleida, Universitat de Lleida, Montserrat  
37 Roig 2, 25008 Lleida, Spain

38 <sup>5</sup> Department of Biological Chemistry, John Innes Centre, Norwich NR4 7UH, United  
39 Kingdom

40 <sup>6</sup> CEA, DSV, IBEB, Laboratoire d'Ecophysiologie Moléculaire des Plantes, Saint-Paul-lez-  
41 Durance, F-13108, France

42 <sup>7</sup>CNRS, UMR 7265 Biologie Végétale & Microbiologie Environnementale, Saint-Paul-lez-  
43 Durance, F-13108, France

44 <sup>8</sup> Aix-Marseille Université, Marseille, F-13284, France

45 <sup>9</sup> Division for Biochemistry, Department for Medical Biochemistry and Biophysics,  
46 Karolinska Institutet, 17177 Stockholm, Sweden

47 <sup>10</sup> Heinrich-Heine-University, Department of Neurology, Medical Faculty, Merowinger Platz  
48 1a, 40225 Düsseldorf, Germany

49 <sup>11</sup> Biochimie et Physiologie Moléculaire des Plantes, Centre National de la Recherche  
50 Scientifique, Institut National de la Recherche Agronomique, Université Montpellier,  
51 Montpellier Cedex 1, France

52 <sup>12</sup> Université de Lorraine, Interactions Arbres - Microorganismes, UMR1136, F-54500  
53 Vandoeuvre-lès-Nancy, France

54 <sup>13</sup> INRA, Interactions Arbres - Microorganismes, UMR1136, F-54280 Champenoux, France

55  
56 † The authors have equally contributed to the work

57 \* Corresponding author: Pascal Rey

58 **Summary:**

59 The unusual multidomain glutaredoxin S17 and its partner, the nuclear factor NF-  
60 YC11/NC2 $\alpha$ , control plant development and flowering time in relation to photoperiod in  
61 *Arabidopsis thaliana*.

62  
63  
64  
65  
66  
67  
68  
69  
70  
71  
72  
73  
74  
75  
76  
77  
78  
79  
80  
81  
82  
83  
84  
85  
86  
87  
88  
89  
90

91 **Footnotes:** This work was funded by ANR JC07\_204825 (N.R. and P.R.), ANR 2010  
92 BLAN\_1616 (N.R., P.R., N.B., S.T., F.G., C.R., J-P.R. and J.G-M.), ANR-BLAN 12-BSV6-  
93 0011 (C.R. and J-P.R.) and the German Research Foundation (DFG, SPP 1710) to C.B.  
94 (BE3259/5-1) and to R.S. (SCHE217/16-1).

95

96 **Corresponding author :** Pascal Rey  
97 CEA, DSV, IBEB, Laboratoire d'Ecophysiologie Moléculaire des Plantes, Saint-Paul-lez-  
98 Durance, F-13108, France  
99 Phone: ++33 442254776  
100 E-mail: pascal.rey@cea.fr

101 **Abstract**

102         Glutaredoxins (GRXs) catalyse the reduction of protein disulfide bonds using  
103 glutathione as a reductant. Certain GRXs are able to transfer iron-sulfur (Fe-S) clusters to  
104 other proteins. To investigate the function of *Arabidopsis thaliana* GRXS17, we applied a  
105 strategy combining biochemical, genetic and physiological approaches. GRXS17 was  
106 localized in the nucleus and cytosol, and its expression was elevated in the shoot meristems  
107 and reproductive tissues. Recombinant GRXS17 bound Fe<sub>2</sub>S<sub>2</sub> clusters, a property likely  
108 contributing to its ability to complement the defects of a yeast strain lacking the mitochondrial  
109 GRX5. However, a *grxs17* knock-out *Arabidopsis* mutant exhibited only a minor decrease in  
110 the activities of Fe-S enzymes, suggesting that its primary function is as a disulfide  
111 oxidoreductase. The *grxs17* plants were sensitive to high temperature and long-day  
112 photoperiod, resulting in elongated leaves, compromised shoot apical meristem, and delayed  
113 bolting. Both environmental conditions applied simultaneously led to a growth arrest. Using  
114 affinity chromatography and split-YFP methods, a nuclear transcriptional regulator termed  
115 NF-YC11/NC2 $\alpha$  was identified as a GRXS17 interacting partner. A mutant deficient in NF-  
116 YC11/NC2 $\alpha$  exhibited similar phenotypes to *grxs17* in response to photoperiod. Therefore,  
117 we propose that GRXS17 interacts with NF-YC11/NC2 $\alpha$  to relay a redox signal generated by  
118 photoperiod to maintain meristem function.

119

120

121

122

123

124

125

126

## 127 **Introduction**

128           Glutaredoxins (GRXs) are small oxidoreductases structurally related to thioredoxins  
129 (TRXs) and present in most organisms (Rouhier et al., 2008; Meyer et al., 2009). Their  
130 capacity to reduce disulfide bonds is usually dependent on glutathione (GSH) and relies on a  
131 4-residue active-site motif comprising at least one redox-active cysteine (Rouhier et al.,  
132 2006). In higher plants, GRXs are encoded by multigene families and subdivided into four  
133 classes (Couturier et al., 2009). GRXs from classes I and II are present in all photosynthetic  
134 organisms and possess in most cases the motifs CPXC and CGFS as active sites, respectively.  
135 GRXs from class III are restricted to terrestrial plants and display a CCXX motif. Class-IV  
136 GRXs are present both in algae and in terrestrial plants and are composed of three domains,  
137 one N-terminal GRX module carrying a CXXC/S motif followed by two domains of unknown  
138 function.

139           Through their biochemical function as disulfide reductases, GRXs are thought to alter  
140 the activity of metabolic enzymes and transcriptional factors (Michelet et al., 2005; Murmu et  
141 al., 2010; Couturier et al., 2014). They also participate in the regeneration of thiol-dependent  
142 antioxidant enzymes (Rouhier et al., 2001; Gama et al., 2007; Tarrago et al., 2009; Couturier  
143 et al., 2011). Besides, other functions have been proposed for class I and II GRXs owing to  
144 their capacity to bind iron-sulphur (Fe-S) clusters (Rouhier et al., 2007; Bandyopadhyay et al.,  
145 2008; Rouhier et al., 2010). For instance, oxidized glutathione promotes Fe-S cluster  
146 disassembly from human GRX2 and restores disulfide reductase activity, therefore class-I  
147 GRXs may constitute redox sensors (Lillig et al., 2005). GRXs belonging to class II, also  
148 named monothiol GRXs, seem intimately linked to iron metabolism. Those present in  
149 mitochondria participate in Fe-S cluster assembly, most likely as Fe-S carriers from scaffold  
150 proteins to acceptor proteins (Rodriguez-Manzanique et al., 2002; Mühlenhoff et al., 2003;  
151 Bandyopadhyay et al., 2008). In addition, nucleo-cytosolic monothiol GRXs participate in  
152 iron sensing and trafficking in yeast and animals (Ojeda et al., 2006; Pujol-Carrion et al.,  
153 2006; Kumanovics et al., 2008; Mühlenhoff et al., 2010; Haunhorst et al., 2013). However, it  
154 is not known if GRXs play a role in Fe-S cluster assembly or iron sensing in plants.

155           Recently, essential roles of plant GRXs have been unveiled in developmental  
156 processes and stress responses. Several *Arabidopsis thaliana* GRXs from class III participate  
157 in the tolerance to photooxidative stress (Laporte et al., 2012) and in defence against  
158 pathogens (Ndamukong et al., 2007; La Camera et al., 2011). Others are required for proper  
159 reproductive development through interaction with bZIP-type TGA transcription factors

160 (Xing and Zachgo, 2008; Murmu et al., 2010). Concerning class-I GRXs, an Arabidopsis  
161 mutant deficient in both GRXC1 and C2 has a lethal phenotype due to impaired embryo  
162 development (Riondet et al., 2012). Among the four class-II GRXs (S14, S15, S16 and S17),  
163 the plastidial S14 isoform participates in arsenic tolerance in a hyper-accumulating fern  
164 (Sundaram et al., 2008) and is induced in response to high temperature in *A. thaliana*  
165 (Sundaram and Rathinasabapathi, 2010). Tomato plants silenced for the expression of  
166 *GRXS16*, encoding another plastid-localized GRX, display increased sensitivity to osmotic  
167 stress (Guo et al., 2010). GRXS14 and GRXS15 are presumed to participate in responses to  
168 oxidative stress (Cheng et al., 2006; Cheng, 2008). Concerning GRXS17, Arabidopsis  
169 knockout plants growing at 28°C exhibited impaired primary root growth, impaired flowering  
170 and altered sensitivity to auxin (Cheng et al., 2011). Consistently, ectopic expression of  
171 Arabidopsis GRXS17 in tomato plants resulted in enhanced thermo-tolerance (Wu et al.,  
172 2012).

173 In this work, we examined the physiological role of Arabidopsis GRXS17, which  
174 belongs to class II and has three CGFS active sites, in relation to its biochemical functions.  
175 Recombinant GRXS17 incorporated Fe<sub>2</sub>S<sub>2</sub> clusters and complemented the yeast *grx5* mutant.  
176 However, in plants, GRXS17 had a minor role in Fe-S cluster metabolism, as the activities of  
177 cytosolic Fe-S-dependent enzymes were not substantially altered in *grxs17* mutant plants. On  
178 the other hand, *grxs17* plants exhibited severe developmental defects as a consequence of a  
179 perturbed shoot meristem, specifically at elevated temperatures and in long-day conditions.  
180 We show that GRXS17 interacts with a nuclear transcriptional factor, NF-YC11/NC2 $\alpha$ , which  
181 is also involved in the control of plant development as a function of photoperiod duration. Our  
182 data indicate that GRXS17 plays an important role in meristem maintenance and suggest that  
183 this role is fulfilled via the relay of a redox-dependent signal to NF-YC11/NC2 $\alpha$ .

184  
185  
186

187 **Results**

188 **Expression of *GRXS17* in Arabidopsis plant organs and subcellular localization**

189 To investigate the function of *GRXS17* *in planta*, we first analyzed its expression  
190 pattern. Previously published quantitative RT-PCR and promoter-GUS fusion data showed  
191 high *GRXS17* expression in growing leaves and anthers of *A. thaliana* (Cheng et al., 2011). To  
192 gain more detail, the GRXS17 protein abundance in various organs was determined using a  
193 serum raised against the whole recombinant protein. The serum specifically recognized a  
194 protein at *ca.* 50 kDa as shown by Western blot analysis of flower protein extracts from WT  
195 and the signal was absent in homozygous *grxS17* plants (Fig. 1A; Fig. S1). GRXS17 was  
196 substantially more abundant in stems, young leaves and flowers. Note that the electrophoretic  
197 mobility of GRXS17 varies in leaf samples due to the proximity of RubisCO, which appears  
198 as a light grey background band in *grxS17* extracts (Fig. 1A-B). *In situ* hybridization was  
199 performed on shoot apical meristem (SAM) and flowers of Arabidopsis WT plants. A strong  
200 digoxigenin staining was found in all meristematic cells, particularly in stem cells (Fig. 1C-  
201 D), and in pollen and ovules (Fig. 1E-F). These data reveal that *GRXS17* is expressed in very  
202 different cell types localized in meristematic areas or in reproductive and vascular organs.

203 In order to determine the subcellular localization of GRXS17, transient expression in  
204 protoplasts and stable expression of *P35S:GRXS17:GFP* fusion were undertaken. The results  
205 indicated that the protein is targeted to both cytosol and nucleus (Fig. 2A-B). The nuclear  
206 localization is surprising considering the absence of a recognizable nuclear localization signal  
207 in GRXS17 sequence and the size of the fusion protein, which should be too big to freely  
208 diffuse through nuclear pores. Therefore, we prepared nuclear and cytosolic fractions from  
209 Arabidopsis inflorescences. Their relative purity was verified using sera against cytosolic and  
210 nuclear markers, TRXh5 (Marchal et al., 2014) and NUC1 (Pontvianne et al., 2010),  
211 respectively. GRXS17 was detected in both fractions in agreement with GRXS17-GFP  
212 localization (Fig. 2C). No signal for GRXS17 was detected in mitochondrial or chloroplastic  
213 extracts (Fig. S2).

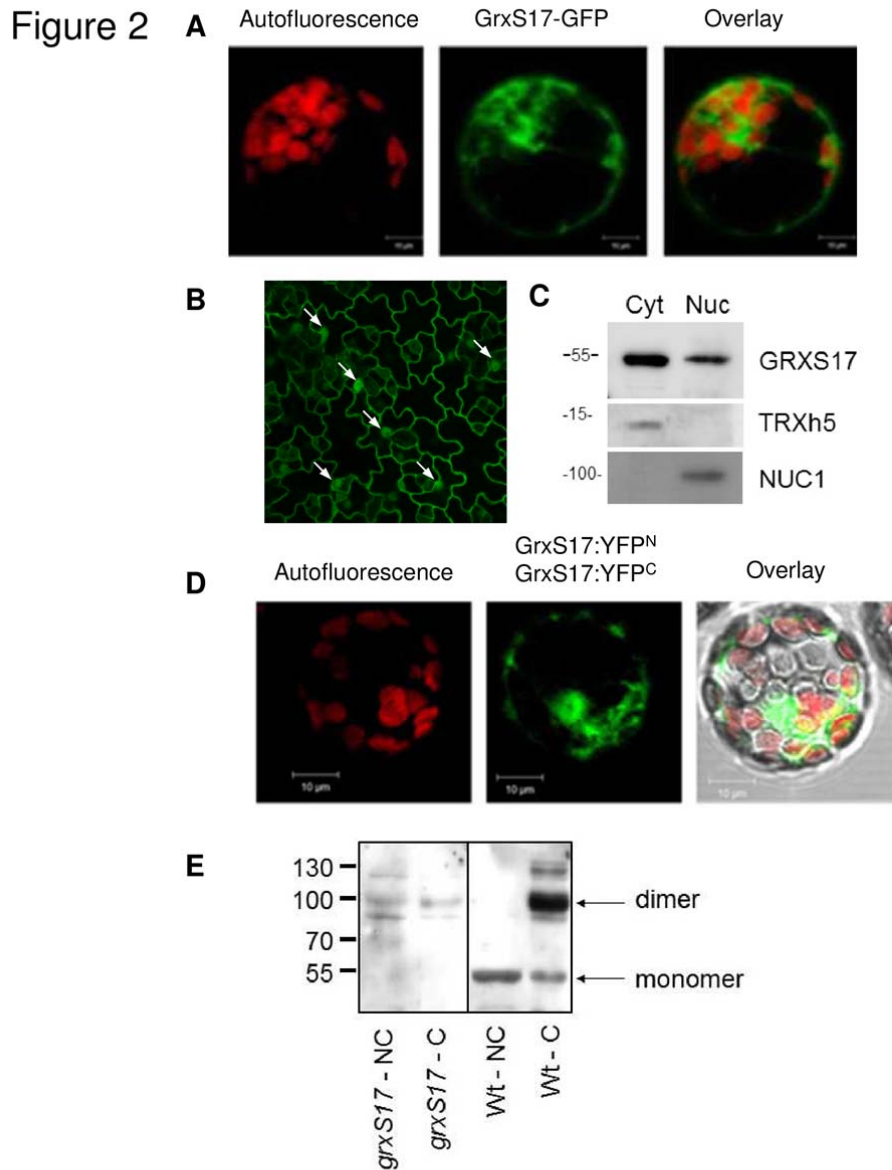


**Figure 2. Subcellular localization and dimerisation of GRXS17.**

(A) Transient expression of a GRXS17:GFP fusion in *A. thaliana* mesophyll protoplasts. Autofluorescence of chlorophyll indicates chloroplasts. (B) Stable expression of a GRXS17:GFP fusion in *Arabidopsis thaliana* leaves. White arrows indicate nuclei. (C) Immunodetection of GRXS17, thioredoxin TRXh5 and nucleolin NUC1 in cytosolic (Cyt) and nuclear (Nuc) extracts of Arabidopsis flower buds. (D) Bimolecular fluorescence complementation assay of GRXS17. Vectors encoding C- and N-terminal split-YFP fusions with GRXS17 were co-transformed into *Arabidopsis thaliana* mesophyll protoplasts. (E) Immunodetection of GRXS17 in *grxS17* and WT extracts cross-linked (C) or not (NC) with DMP.

214            Using bimolecular fluorescence complementation (BiFC) *i.e.*, transient expression of  
 215 two GRXS17 constructs fused to half YFPs in *Arabidopsis* protoplasts, we observed YFP  
 216 signal confirming the nucleo-cytosolic localization and indicating that GRXS17 forms dimers  
 217 in both compartments (Fig. 2D, Fig. S3). The ability of GRXS17 to dimerise *in vivo* was

Figure 1

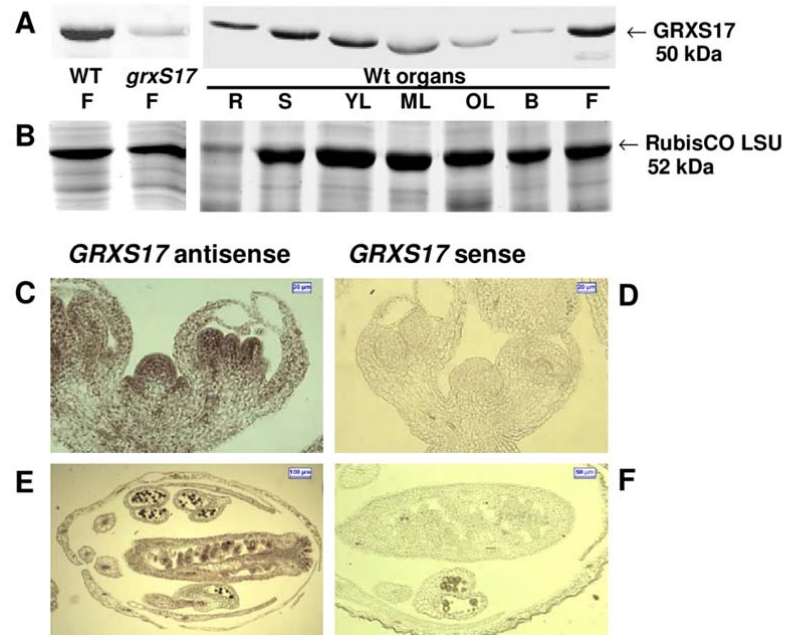


**Figure 1. Expression of *GRXS17* in *A. thaliana* plants.**

(A-B) Western analysis of *GRXS17* abundance. (A) Western blot analysis in flowers from WT and *grxS17* plants, and in organs of WT plants grown under standard conditions (20  $\mu$ g per lane). The RubisCO large subunit (LSU) appears as a light grey background band in the *grxS17* lane. R, root from adult plant; S, stem from bolting plant; YL, young leaf; ML, mature leaf; OL, old leaf; B, floral bud; F, flower. (B) Loading controls: Coomassie blue stained gels (50-kDa region). (C-F) RNA *in situ* hybridization. Longitudinal sections of WT meristem inflorescences (C, D) and flower buds (E, F). Hybridizations were performed with antisense (C, E) or sense (D, F) *GRXS17* cDNA probes.

218 further investigated in crude leaf extracts incubated with the cross-linker dimethyl  
219 pimelimidate•2 HCl (DMP). Upon non-reducing SDS-PAGE and Western blot analysis, a  
220 single band at 50 kDa was apparent in untreated WT samples and an additional 100-kDa

221 band, corresponding to a GRXS17 dimer, was specifically observed in the cross-linked extract  
222 (Fig. 2E). These data indicate that the GRX dimer is not formed via disulfide bridging.

223

#### 224 **Development of the *grxS17* mutant in response to photoperiod**

225 To analyse the physiological function of AtGRXS17, we isolated homozygous *grxS17*  
226 knockout plants from the Arabidopsis SALK\_021301 line (Fig. S1) and transformed this line  
227 with the *GRXS17* cDNA under the control of the CaMV-35S promoter. Two independent  
228 *grxS17 GRXS17* complemented lines, termed 3.3 and 17.8, were generated and transgene  
229 expression was confirmed at the protein level (Fig. S1). The phenotype characteristics of  
230 *grxS17* mutant and complemented lines were investigated under various light and temperature  
231 conditions. When cultivated under standard conditions (22°C/18°C regime, 8-h photoperiod  
232 and 200  $\mu\text{moles photons m}^{-2} \text{ s}^{-1}$ ), all lines showed a similar development (Fig. 3A). Transfer  
233 of 2.5-week old seedlings to 28°C and standard light for 2.5 weeks strongly impaired  
234 development of all genotypes, which displayed thin and elongated leaves. In addition, the  
235 *grxS17* mutant failed to form new leaves, which was partially or entirely complemented in  
236 lines 3.3 and 17.8, respectively (Fig. 3B). These data indicate that GRXS17 is required for  
237 maintenance of the shoot apical meristem at high temperature, consistent with the previously  
238 reported thermo-sensitivity of the *grxS17* line (Cheng et al., 2011).

239           When plants were grown at 22°C and moderate light, but under long-day photoperiod  
240 (16/8h), we observed that 4-week old *grxS17* plants displayed elongated and thickened lamina  
241 (Fig. 3C). The development of the main floral spike (raceme) was delayed, which entirely  
242 failed to form when plants were shifted to continuous light (Fig. 3D). To analyse whether the

243 phenotype appearance is due to day length or related to the total light inception, plants grown  
244 for 2 weeks under standard conditions were transferred to high light ( $500 \mu\text{mol photons m}^{-2}$   
245  $\text{s}^{-1}$ ),  $22^\circ\text{C}$  and short-day conditions. After 3 weeks, there was no change in *grxS17*  
246 development in this light regime (Fig. S4A), indicating that photoperiod duration is the

247 primary determinant for the observed phenotype. When plants were grown under the same  
248 high light intensity under long days, *grxS17* exhibited strongly impaired development (Figs.  
249 S4B, S5G). It is worth mentioning that the temperature measured at the plant level is elevated  
250 by 2°C (24°C) in high-light conditions, thus possibly explaining the more severe phenotype in

Figure 3

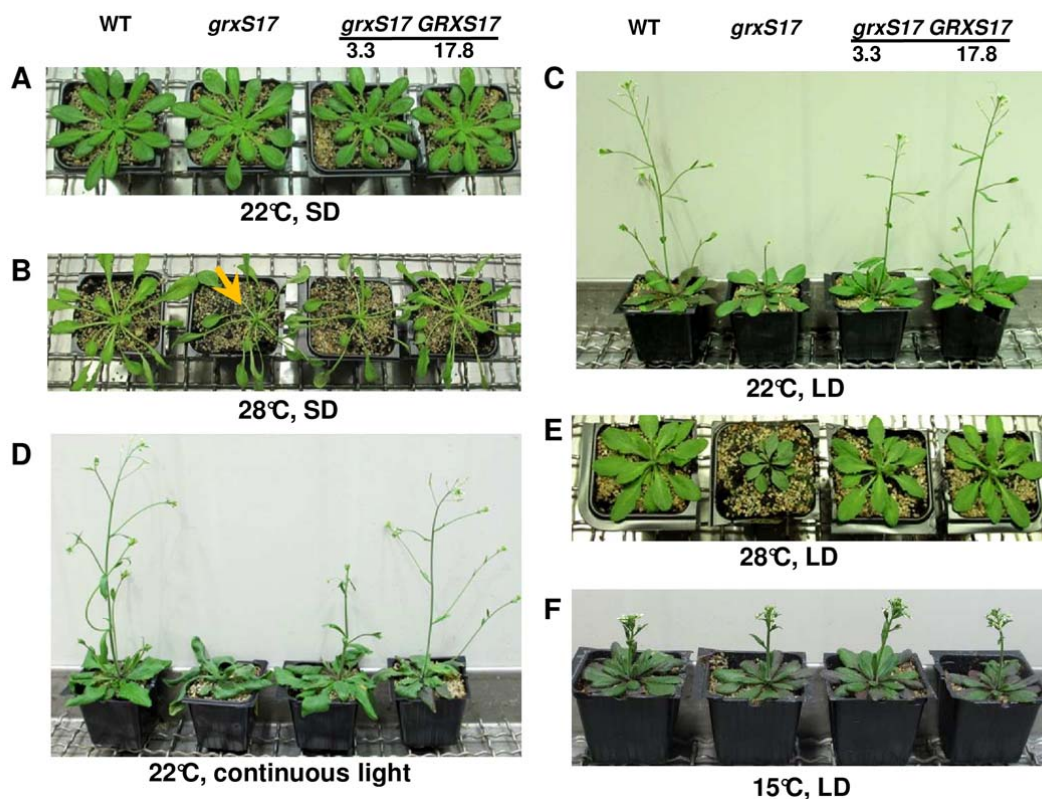


**Figure 3. Growth and development of plants modified in *GRXS17* expression as a function of photoperiod and temperature.**

(A) Five-week old plants grown in standard conditions (8-h photoperiod,  $200 \mu\text{mol photons.m}^{-2}.\text{s}^{-1}$ ) at  $22^\circ\text{C}$ . (B) Plants grown for 2.5 weeks in standard conditions and transferred to  $28^\circ\text{C}$  (8-h photoperiod,  $200 \mu\text{mol photons.m}^{-2}.\text{s}^{-1}$ ) for 2.5 weeks. The arrow indicates the absence of young leaves. (C) Plants grown in long-day photoperiod conditions (16 h,  $200 \mu\text{mol photons.m}^{-2}.\text{s}^{-1}$ ) at  $22^\circ\text{C}$ . (D) Plants grown for 2 weeks in standard conditions and transferred to continuous light ( $200 \mu\text{mol photons.m}^{-2}.\text{s}^{-1}$ ,  $22^\circ\text{C}$ ) for 3 weeks. (E) Plants grown for 2 weeks in standard conditions and transferred to  $28^\circ\text{C}$  and long-day photoperiod (16 h,  $200 \mu\text{mol photons.m}^{-2}.\text{s}^{-1}$ ) for 2.5 weeks. (F) Plants grown for 3 weeks in standard conditions and transferred to  $15^\circ\text{C}$  and long-day photoperiod (16 h,  $200 \mu\text{mol photons.m}^{-2}.\text{s}^{-1}$ ) for 4 weeks. WT, Wild-type plants; *grxS17*, homozygous SALK\_021301 plants; *grxS17 GRXS17* 3.3 and 17.8, two independent *grxS17* lines expressing *GRXS17*. SD and LD, short (8 h) and long (16 h) day.

251 long day at high light compared to moderate light. Under this light regime, there was no  
 252 visual evidence of photooxidative damage in *grxS17* leaves (Fig. S4B). This was confirmed  
 253 by autoluminescence imaging (Fig. S6), which allows recording of the photon emission  
 254 associated with lipid peroxidation (Havaux et al., 2006). When combining high temperature

255 and long day, we observed that *grxS17* growth stopped after a few days (Fig. 3E).  
256 Noteworthy, the growth and reproductive development of *grxS17* plants cultivated for 4  
257 weeks in long-day conditions at 15°C was not modified (Fig. 3F). Similarly, when young  
258 plants were transferred to long-day conditions at 15°C and high light (500  $\mu\text{mol photons m}^{-2}$   
259  $\text{s}^{-1}$ ), no alteration was noticed in *grxS17* (Fig. S4C). Altogether, these data reveal that plants  
260 deficient in GRXS17 display sensitivity to a long-day regime in a temperature-dependent  
261 manner.

262 When *grxS17* plants were grown under long-day and high-light conditions, a  
263 significant delay of bolting was observed. These plants only formed secondary floral spikes  
264 after some time (Fig. S5B, D, F and G). In short-day conditions, floral development was even  
265 accelerated (Fig. S5A, C and E), while *grxS17* vegetative growth was not affected.  
266 Complemented lines exhibited contrasting phenotypes under short day, one line (3.3)  
267 flowering like the mutant and the other (17.8) like WT. The difference could originate from  
268 the much higher GRXS17 amount in the latter (Fig. S1). Collectively, these data point to the  
269 central role of GRXS17 in conveying environmental variations, such as temperature and day  
270 length, to coordinate the flowering response in plants.

271

272 **The shoot apical meristem is compromised in the *grxS17* mutant**

273           As floral induction depends on the transition of the shoot apical meristem (SAM) from  
274 vegetative to reproductive fate (Levy and Dean, 1998), we performed histological analysis of  
275 SAM in *grxS17* mutants. The SAM overall structure was not altered in the mutant grown in  
276 short-day conditions (Fig. S7). On the contrary, when grown under long days, the meristem

277 area was smaller in *grxS17* compared to WT (Fig. 4A). The cell numbers in L1, L2 and L3  
278 layers were 45% lower in *grxS17* than in WT, revealing impairment in the division of stem  
279 cells (Fig. 4C). Moreover, the size of meristematic cells was noticeably increased in the  
280 mutant (Fig. 4A), suggesting that the lower cell division rates are associated with increased

281 cell expansion. These changes in meristematic cell size and numbers are consistent with the  
282 high *GRXS17* expression level observed in the meristem (Fig. 1C) and likely lead to the  
283 impaired development of *grxS17* plants observed under conditions of long-day photoperiod  
284 and/or high temperature (Fig. 3; Fig. S5). Histological analysis of mesophyll cells in plants

Figure 4

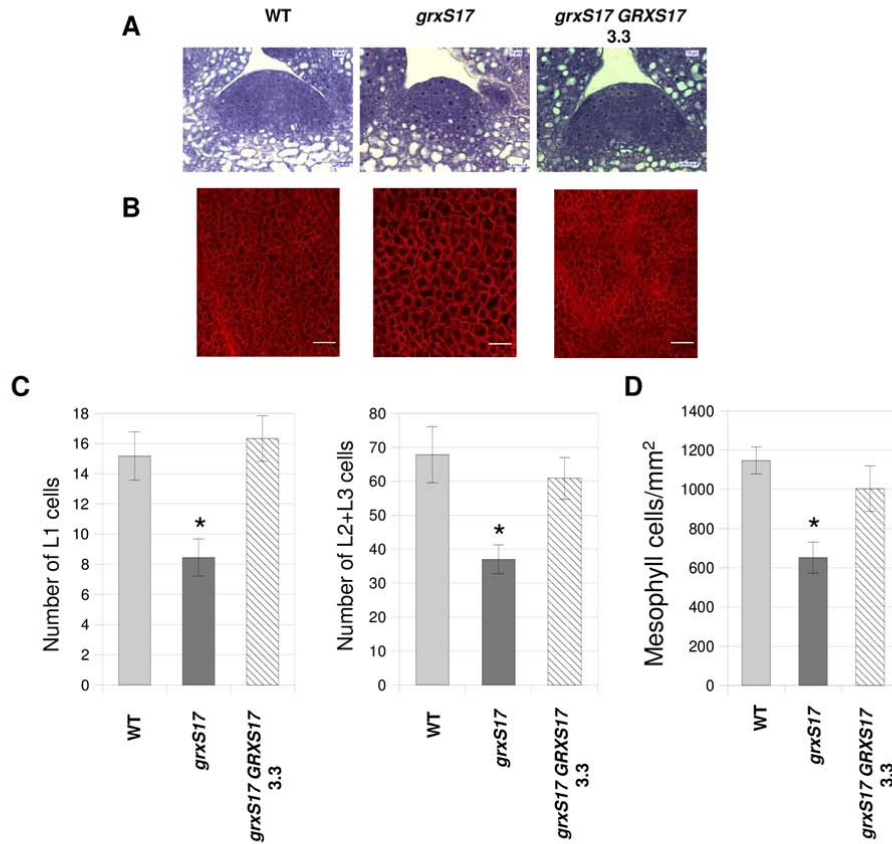


**Figure 4. Structure of shoot apical meristem (SAM) and leaves in *grxS17* plants.**

(A) Histological structure of the SAM stained by toluidine blue in 7-day old wild-type, *grxS17* and *grxS17 GRXS17* (line 3.3) plants grown in long-day conditions (16 h) and high light (500  $\mu\text{mol photons.m}^{-2}.\text{s}^{-1}$ ). (B) Observation of mesophyll cells in leaves of 3-week old plants grown under long-day/high-light conditions. (C) Number of L1, L2 and L3 layer stem cells in SAM cross-sections shown in (A). Ten sections per genotype were analyzed. (D) Density of mesophyll cells in the sections shown in (B) (n: 12). \*, value significantly different from Wt value with  $p < 0.05$  (t-test).

285 grown under long-day and high-light conditions revealed a reduced cell density in mutant  
 286 plants ( $652 \pm 79 \text{ cells.mm}^{-2}$ ) compared to WT ( $1148 \pm 68 \text{ cells.mm}^{-2}$ ) and a much larger cell  
 287 size (Fig. 4B, D). These data indicate that GRXS17 is required for cell division under long-  
 288 day conditions.

289

## 290 **AtGRXS17 architecture and capacity to bind Fe-S clusters**

291 To investigate the biochemical function of AtGRXS17, and how this could affect  
292 meristem development, we first analyzed the capacity of the protein to bind Fe-S clusters. *A.*  
293 *thaliana* GRXS17 possesses an N-terminal TRX-like domain with a WCDAS motif in place  
294 of the canonical WCGPC active site, followed by three GRX domains containing CGFS  
295 motifs (Fig. 5A). This architecture is unique to land plants, since mammalian, fungal and algal  
296 homologs consist of one TRX and maximally two GRX domains (Couturier et al., 2009). The  
297 GRX modules of GRXS17 share 62 to 65% identity and are subsequently referred to as M2,  
298 M3 and M4. From secondary structure prediction and 3D-structure modeling, the four  
299 AtGRXS17 domains all adopt a classical TRX fold and are connected by long linker  
300 sequences (Fig. S8). The capacity of recombinant AtGRXS17 to incorporate Fe-S clusters like  
301 other Arabidopsis CGFS GRXs (Bandyopadhyay et al., 2008) was analyzed after anaerobic *in*  
302 *vitro* reconstitution mediated by the cysteine desulfurase IscS in the presence of glutathione.  
303 Indeed, upon purification of GRXS17, the oxygen-sensitive Fe-S clusters are lost; therefore  
304 reconstitution of the clusters guarantees a sufficient amount of holo-GRXS17 for  
305 spectroscopy analysis. The UV-visible spectrum of the reconstituted GRXS17 showed  
306 absorbance peaks at 320 nm and around 420 nm similar to other Fe-S cluster coordinating  
307 GRXs and typical for Fe<sub>2</sub>S<sub>2</sub> clusters (Fig. 5B). Estimation of the iron content in a freshly  
308 reconstituted WT protein indicated the presence of  $2.48 \pm 0.58$  Fe atoms/monomer. To  
309 investigate the contribution of each domain to cluster binding, the active-site cysteines were  
310 replaced by serines, either individually or in all three GRX domains. Whereas the triple-Cys  
311 mutant (C179/309/416S) did not incorporate any Fe-S cluster upon *in vitro* reconstitution,  
312 variants carrying one single substitution all incorporated between 40 to 60% of clusters as  
313 assessed by relative absorbance measurements at 420 nm (Fig. 5C). Since each of the active  
314 site cysteines of the GRX-subunits contributed to Fe<sub>2</sub>S<sub>2</sub> incorporation, these data - together  
315 with the quantification of Fe - indicate that AtGRXS17 dimers incorporate three Fe<sub>2</sub>S<sub>2</sub>  
316 clusters *in vitro*, involving each GRX domain. Furthermore, the stoichiometry indicates that  
317 the GSH included in the reconstitution assay acts as a Fe-S cluster ligand as described for all  
318 other CGFS GRXs.

319

## 320 ***A. thaliana* GRXS17 rescues most yeast *grx5* mutant phenotypes**

Figure 5

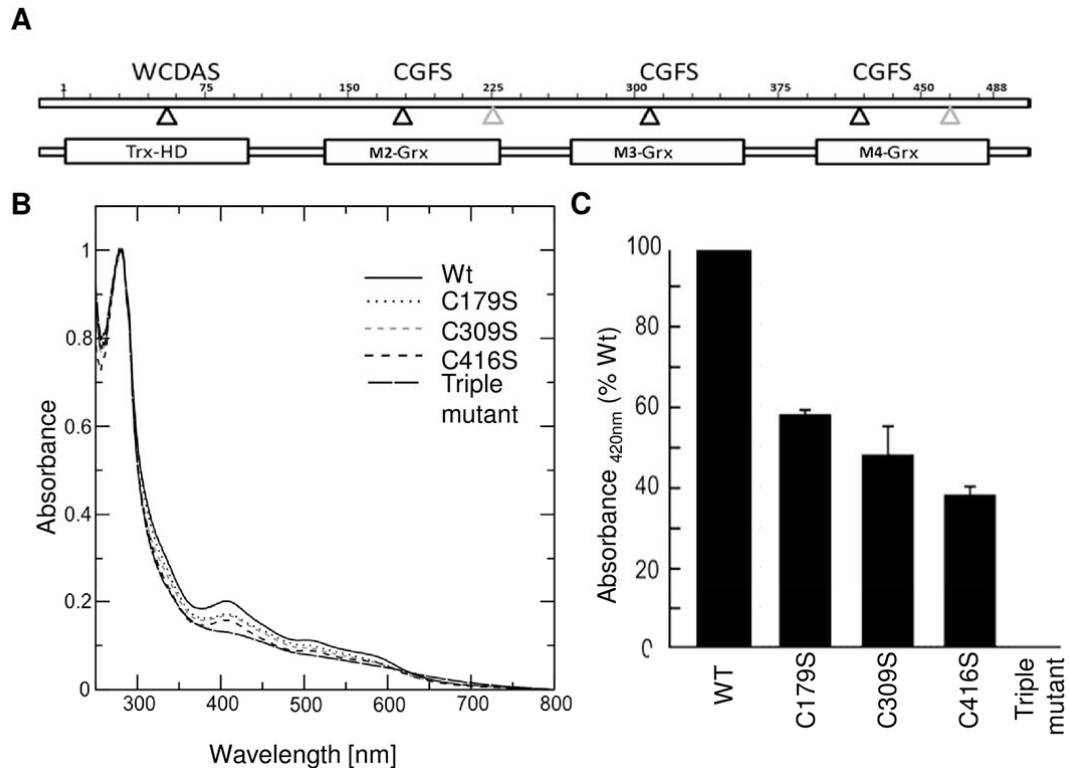


**Figure 5. Incorporation of Fe-S clusters into recombinant WT and mutated AtGRXS17.** (A) Domain structure of GRXS17. TRX-HD: TRX-like homology domain; M2-GRX, M3-GRX and M4-GRX: three monothiol-GRX domains. Positions of active-site cysteines are indicated by black triangles and that of other cysteine by a grey triangle. (B) Absorption spectra of GRXS17 and cysteine mutants. UV-visible absorption spectra were recorded immediately after *in vitro* reconstitution in anaerobic conditions. The active-site cysteines of each GRX domain were individually or together substituted by serines (M2:C179S; M3: C309; M4: C416S; C179/309/416S). (C) Relative absorption at 420 nm of GRXS17 mutants.

321 To further investigate a possible role of GRXS17 as a Fe-S cluster carrier, its capacity  
322 to rescue the defects of a yeast *grx5* mutant was examined. The entire protein or the three  
323 individual GRX domains were fused to the Grx5 mitochondrial targeting sequence and a C-  
324 terminal haemagglutinin (HA) tag. The constructs were expressed in Baker's yeast,

Figure 6

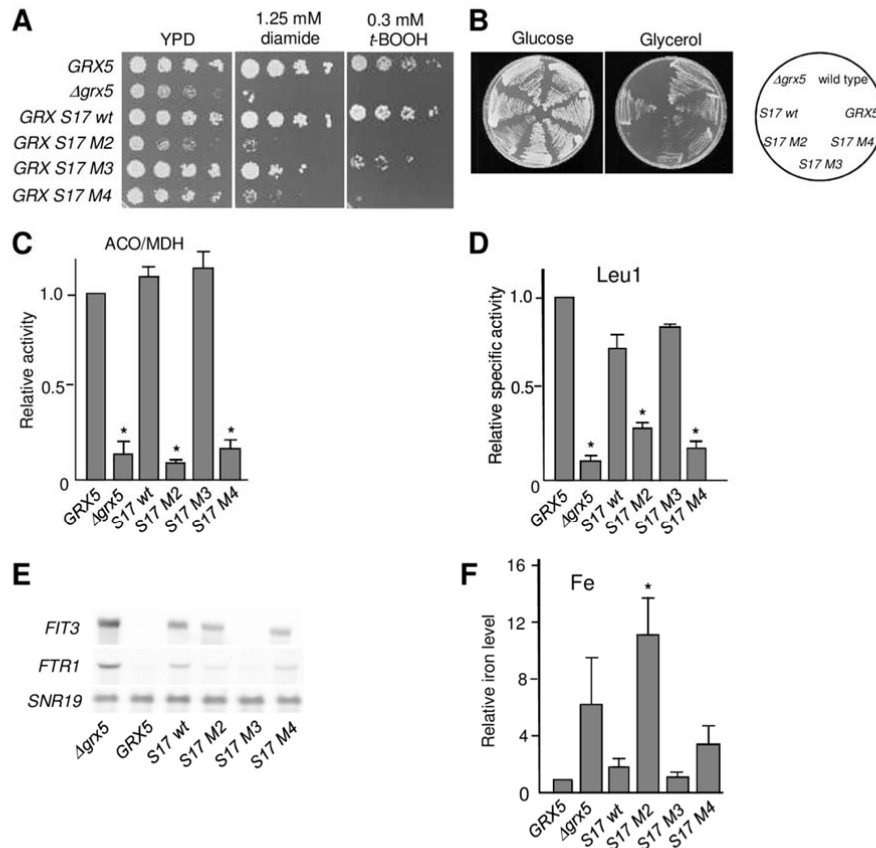


**Figure 6. Rescue of the *S. cerevisiae grx5* mutant defects by *AtGRXS17*.**

(A) Sensitivity to *t*-BOOH or diamide after 3 days at 30°C on YPD plates. (B) Growth on glucose (YPD plates) or glycerol (YPGly plates) after 3 days at 30°C. (C) Relative ratio between aconitase and malate dehydrogenase activities, normalized with respect to the ratio in the WT strain, in exponential cultures at 30°C in YPGalactose medium. (D) Relative specific Leu1 activity. (E) Northern blot analysis of *FIT3* and *FTR1* mRNA levels from exponential cultures at 30°C. Loading control: *SNR19* mRNA. (F) Relative iron content from exponential cultures at 30°C in YPD medium. Mean  $\pm$  SD (n: 3). Asterisks indicate statistically significant differences (Student's *t*-test,  $p < 0.05$ ) compared to WT (*GRX5*) cultures.

325 *Saccharomyces cerevisiae* and the localization of the Arabidopsis proteins in the  
 326 mitochondrial matrix was confirmed by Western blot analysis (Fig. S9). Phenotype studies  
 327 indicated that only the entire protein (WT), and the M3 module to a lesser extent, rescued the  
 328 sensitivity to two externally added oxidants, for which yeast *grx5* mutant cells are

329 hypersensitive (Rodriguez-Manzaneque et al., 2002), *tert*-butyl hydroperoxide (*t*-BOOH,  
330 causing general oxidative damage on cellular macromolecules) and diamide (specific oxidant  
331 of thiol groups) (Fig. 6A). When grown under obligate respiratory conditions (glycerol as  
332 carbon source), both the M3 and M4 modules, in addition to the entire GRXS17 molecule,  
333 totally or partially rescued the *S. cerevisiae grx5* defective phenotype (Fig. 6B). The M3  
334 module also fully rescued, like GRXS17, the ability to express active aconitase holoenzyme  
335 (Fig. 6C) and mostly restored isopropylmalate isomerase (Leu1) activity (Fig. 6D). These  
336 two Fe-S containing enzymes are located in mitochondria and cytosol, respectively, and both  
337 are dependent on the mitochondrial Fe-S cluster assembly pathway. We then checked the  
338 expression of iron uptake genes by determining the transcript levels of two reporter genes of  
339 the Aft1 regulon, *FTR1* and *FIT3*. Of the three modules, only M3 restored repression of both  
340 genes in *grx5* cells, while the entire GRXS17 molecule was unable to repress *FTR1* and *FIT3*  
341 expression (Fig. 6E), indicating that one component participating in iron status signalling is  
342 still deficient and that this could be due to some steric incompatibility linked to the modular  
343 architecture of GRXS17. Accordingly, the M3 domain suppressed iron accumulation in *grx5*.  
344 Of note, expression of the entire GRXS17 protein also prevented iron accumulation (Fig.  
345 6F). To summarize, the entire AtGRXS17 rescued most *grx5* phenotypes, notably the  
346 activities of Fe-S containing enzymes.

347

348 **GRXS17 plays a minor role in maintaining the activity of cytosolic Fe-S enzymes**

349           Next, we investigated whether GRXS17 fulfils a role in Fe-S cluster assembly in *A.*  
350 *thaliana*. Therefore, activities and/or abundance of Fe-S enzymes were analyzed, including  
351 aconitases (one Fe<sub>4</sub>S<sub>4</sub>), aldehyde oxidases (two Fe<sub>2</sub>S<sub>2</sub>, FAD and molybdenum cofactors) and  
352 photosystem I (PSI, three Fe<sub>4</sub>S<sub>4</sub>). All measurements were performed using 2-week old

353 seedlings grown under conditions where mild phenotypic changes are visible (22°C and 16-h  
354 light) or under conditions leading to severely impaired growth in *grxS17* (plants shifted to  
355 28°C, 16-h light) (Fig. S10A). Two mutant alleles of *ATM3* (*ABC TRANSPORTER OF THE*  
356 *MITOCHONDRIA 3/ABCB25*), encoding a transporter that provides persulfide for cytosolic

357 Fe-S cluster assembly (Schaedler et al., 2014) were used for comparison. The *atm3-1* and  
358 *atm3-4* mutants are strong and weak mutant alleles, respectively, that have significantly  
359 decreased activities of aldehyde oxidases and cytosolic aconitase (Bernard et al., 2009).  
360 Protein extracts from leaf samples were separated by native gel electrophoresis, followed by

Figure 7

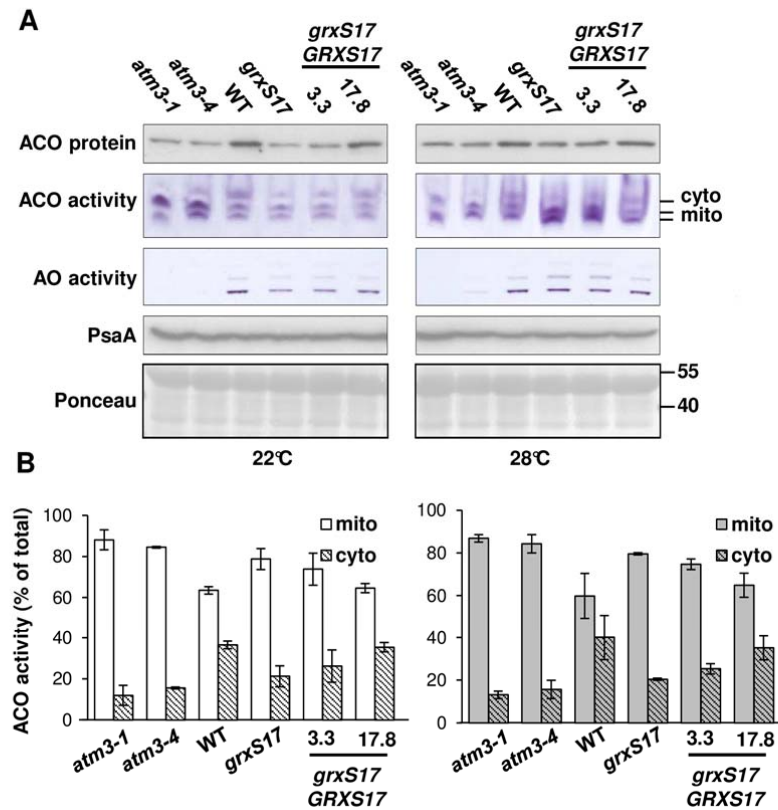


**Figure 7. Activities and levels of Fe-S enzymes in plants modified in *GRXS17* expression.** Wild type (WT), a *grxS17* knock-out mutant and two complemented lines (3.3 and 17.8) were grown for 14 days under standard conditions (22°C) or transferred to 28°C after 7 days (Fig. S10). Mutant alleles in the *ABC Transporter of the Mitochondria 3* (*atm3-1* and *atm3-4*) were used for comparison. (A) Activities of aconitase (ACO) and aldehyde oxidase (AO) isozymes visualized as a formazan precipitate in a native gel assay. Cytosolic (cyto) and mitochondrial (mito) isoforms of ACO are indicated. Equal protein amounts (160 µg for ACO and 60 µg for AO) were loaded per lane. Immunoblotting of ACO and PsaA (a subunit of PSI) in Arabidopsis seedlings (10 µg protein per lane) and loading control (Ponceau). (B) Relative activities of cytosolic and mitochondrial aconitase isoforms quantified using ImageJ software. The values are given as percentages of the sum of the band intensities per lane (mean ± SD). The data are representative of 3 independent experiments.

361 in-gel activity staining. Part of the same protein extract was subjected to denaturing SDS-  
 362 PAGE and Western blotting to estimate protein levels of aconitase and PSI. As expected for a  
 363 cytosolic protein, *GRXS17* is not required for the maturation of mitochondrial (aconitases)

364 and plastidial (photosystem I) Fe-S proteins (Fig. 7A). In *grxS17* plants grown at 22°C, the  
365 amount of total aconitase protein was approximately 40% of WT, corresponding to a similar  
366 decrease in activity of the cytosolic isoform (Fig. 7A-B). Aldehyde oxidase activity was  
367 decreased to ca. 50% in *grxS17* at this temperature, compared to less than 5% in *atm3-4* (Fig.  
368 7A, left panel; Fig. S10B). In the complemented 3.3 line, the activities at 22°C of cytosolic  
369 aconitase and aldehyde oxidase were partially restored, and fully restored in the 17.8 line. In  
370 *grxS17* plants grown at 28°C, the activities of the mitochondrial aconitase isoforms was  
371 increased and total aconitase protein levels were close to WT levels (Fig. 7A-B, right panels).  
372 Further, there was no difference in aldehyde oxidase activity at this temperature (Fig. S10B,  
373 right panel). In comparison with the *atm3* alleles, neither of which is a knock-out, the *grxS17*  
374 knock-out mutant displayed a relatively moderate decrease in cytosolic Fe-S enzymes in  
375 environmental conditions that lead to strongly impaired development. Taken together, these  
376 data suggest that GRXS17, despite its capacity to bind Fe-S clusters *in vitro* and to rescue the  
377 yeast *grx5* mutant, does not play a critical function in *de novo* synthesis of Fe-S clusters *in*  
378 *planta*.

379

### 380 **Identification of a nuclear factor interacting with GRXS17**

381 To explore other possibilities for how GRXS17 functions in meristem development, we  
382 performed affinity chromatography using a Ni-matrix loaded with His-tagged GRXS17 to  
383 identify interacting proteins. After applying a crude leaf extract, the bound proteins were  
384 eluted with DTT, and identified by mass-spectrometry. A number of proteins were repeatedly  
385 isolated in 15 independent affinity experiments (Table I). Interestingly, the predicted or  
386 experimentally determined localization of most proteins, *e.g.* cytosol or nucleus, is  
387 comparable to that of GRXS17. In accordance with a role of GRXS17 in redox signaling  
388 pathways and with the known interaction of GRX3/PICOT with protein kinase C in animal  
389 cells, one transcription factor and one kinase were identified. The At3g12480 gene product,  
390 NF-YC11/NC2 $\alpha$ , isolated in 7 out of 15 experiments, displayed high peptide sequence  
391 coverage. This partner was selected for deeper investigations because proteins of the NF-Y  
392 family are known nuclear factors regulating developmental processes (Kumimoto et al.,  
393 2010). Transient expression of NF-YC11/NC2 $\alpha$ -GFP in *A. thaliana* protoplasts indicated that  
394 the protein is localized both in cytosol and nucleus (Fig. 8A), like GRXS17. The interaction  
395 between both proteins was further confirmed using BiFC exclusively in the nucleus (Fig. 8B;  
396 Fig. S3).

Figure 8

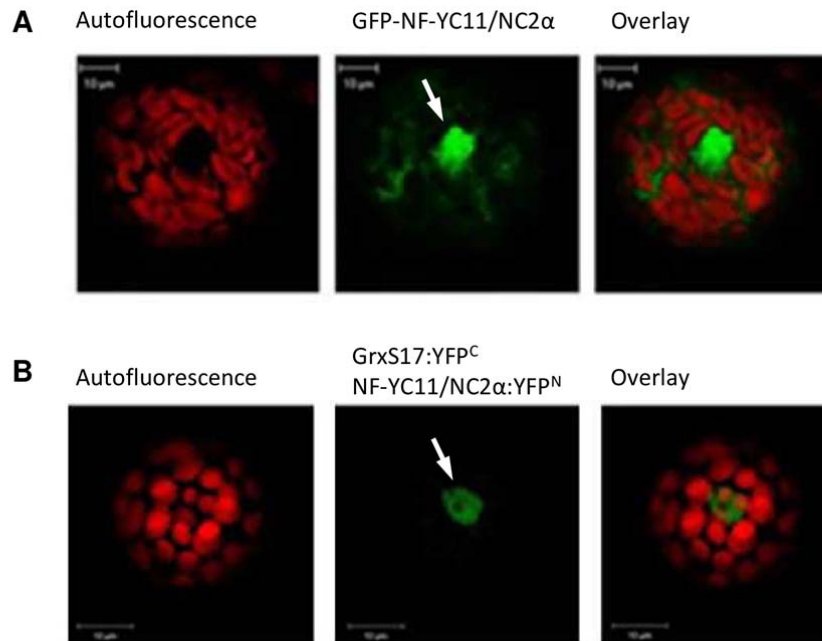


**Figure 8. Localisation of NF-YC11/NC2α and interaction with GRXS17.** Isolated *A. thaliana* mesophyll protoplasts were transiently transformed with a NF-YC11/NC2α:GFP fusion (A) or with split-YFP constructs containing GRXS17 or NF-YC11/NC2α (B). White arrows indicate nuclei.

397

398 **Development of *nf-yc11/nc2α* plants as a function of photoperiod**

399 We isolated knockout plants for *NF-YC11/NC2α* expression from the GABI-Kat 042E02  
400 line (Kleinboelting et al., 2012), and only 4% as opposed to the expected 25% homozygous

Figure 9

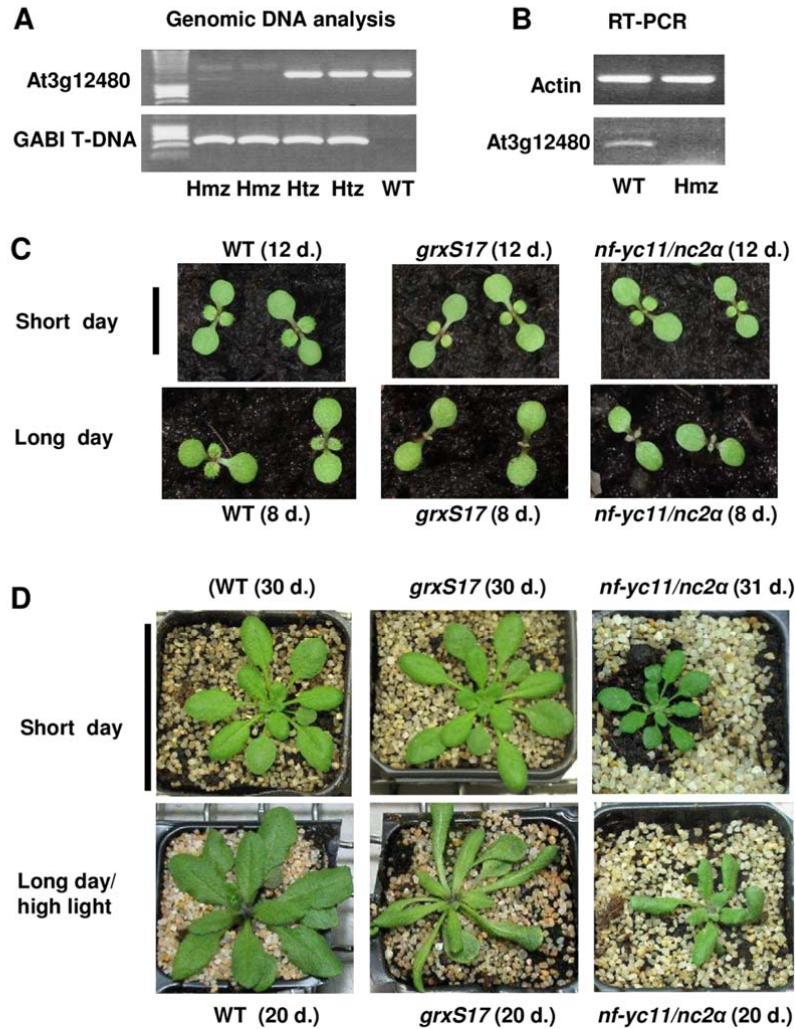


**Figure 9. Characterization of a *nf-yc11/nc2a* mutant and comparison of the growth of *grxS17* and *nf-yc11/nc2a* plants as a function of photoperiod duration.**

(A) PCR analysis of genomic DNA of At3g12480 and T-DNA in WT, heterozygous (Htz) and homozygous (Hmz) plants of the GABI-042E02 mutant line. (B) RT-PCR analysis of WT and homozygous plants. (C) Seedling development in short- and long-day conditions (8- and 16-h, respectively) at moderate light ( $200 \mu\text{mol photons m}^{-2} \text{s}^{-1}$ ) and  $22^\circ\text{C}$ . The seedlings were grown simultaneously in the same conditions and the original photographs are shown in Fig. S 11. (D) Vegetative growth of plants in standard light conditions (short-day: 8-h photoperiod and moderate light,  $200 \mu\text{mol photons m}^{-2} \text{s}^{-1}$ ) and in long-day and high-light conditions (16-h photoperiod,  $500 \mu\text{mol photons m}^{-2} \text{s}^{-1}$ ) at  $22^\circ\text{C}$ . The plant age is indicated for each genotype and culture condition. Scale bars: 1 and 6 cm in C and D, respectively.

401 *nf-yc11/nc2a* plants were recovered in the T2 progeny (Fig. 9A-B). When grown under short-  
 402 day conditions and moderate light, *nf-yc11/nc2a* plants showed slow and altered development  
 403 with a compact rosette, small leaves and a disorganized floral spike (Fig. 9D; Fig. S11C). We  
 404 transferred 33-day old *nf-yc11/nc2a* plants grown in short-day to long-day conditions and

405 observed a strongly reduced development of the main spike and many secondary  
406 inflorescences compared to WT (Fig. S11C; Fig. 3C). We then compared the development of  
407 WT, *nf-yc11/nc2α* and *grxS17* seedlings under short- and long-day conditions (Fig. 9C). We  
408 did not observe any difference in germination and cotyledon development for the three  
409 genotypes in both photoperiod conditions. While in short-day photoperiod, the first two leaves  
410 appeared at the same time in the three lines, the development of these two leaves was  
411 substantially delayed in *nf-yc11/nc2α* and *grxS17* plants in long-day conditions (Fig. 9C). We  
412 analyzed the phenotype of *nf-yc11/nc2α* plants following sowing in long-day photoperiod and  
413 high-light conditions. We observed that growth and development of these plants were more  
414 perturbed than in control conditions (Fig. 9D). Particularly, *nf-yc11/nc2α* plants remained  
415 much smaller than WT and *grxS17* plants. They exhibited elongated and distorted leaves, a  
416 trait characteristic shared by the *grxS17* mutant. In these long-day conditions, no main floral  
417 spike was observed and only secondary small spikes developed (Fig. S11C). Taken together,  
418 these observations indicate that NF-YC11/NC2α participates in plant developmental processes  
419 in relation to the photoperiod duration and reveal that *nf-yc11/nc2α* and *grxS17* plants share  
420 similar developmental characteristics in long-day conditions.

421  
422  
423  
424  
425

426 **Discussion**

427 **Physiological function of GRXS17 in relation to its biochemical properties**

428 In this work, we showed that GRXS17 is a central element for plant development in  
429 relation to environmental factors such as photoperiod and temperature and we investigated  
430 whether a major function in Fe-S protein biogenesis may underpin its physiological role.  
431 Previous studies indicated that multi-domain GRX orthologs from yeast and vertebrates bind  
432 Fe-S clusters and modify the activity of iron-responsive transcriptional regulators (Ojeda et  
433 al., 2006; Pujol-Carron et al., 2006; Kumanovics et al., 2008; Mercier and Labbé 2009; Jbel et  
434 al., 2011), affecting the intracellular iron distribution through the maturation of most iron-  
435 containing proteins (Mühlenhoff et al., 2010; Haunhorst et al., 2013). Accordingly, we  
436 showed that AtGRXS17 is able to bind Fe<sub>2</sub>S<sub>2</sub> clusters by *in vitro* reconstitution experiments  
437 and to complement the defects in Fe-S cluster maturation of the *S. cerevisiae grx5* strain (Figs  
438 5-6). However, we found that GRXS17 in *A. thaliana* does not play a major role in Fe-S  
439 protein biogenesis. Although *grxS17* seedlings do have decreased activities of cytosolic  
440 aconitase and aldehyde oxidases in control conditions (Fig. 7), the effect is far less severe than  
441 that observed in the *atm3* mutant lines (Bernard et al., 2009). Moreover, the aldehyde oxidase  
442 activity, which depends on two Fe<sub>2</sub>S<sub>2</sub> clusters, is not decreased in *grxS17* plants at 28°C, a  
443 temperature condition leading to a severe phenotype. Therefore, our data indicate that  
444 GRXS17 is not involved in *de novo* biosynthesis of cytosolic Fe<sub>2</sub>S<sub>2</sub> clusters, in agreement  
445 with the viability of the knock-out mutant. Indeed, because many cytosolic and nuclear Fe-S  
446 proteins are essential, mutants in Fe-S cluster assembly are generally embryo lethal (Balk and  
447 Schaedler, 2014). An alternative explanation is that the function of GRXS17 is redundant or is  
448 compensated by another component of the Fe-S cluster assembly pathway. However, as  
449 GRXS17 is the only class-II GRX present in cytosol and nucleus, it is unlikely that such a  
450 function is fulfilled by another GRX. Taking into consideration the *in vitro* capacity of  
451 GRXS17 to bind Fe-S clusters and the variations observed in aconitase activity in *grxS17*  
452 plants, we can speculate that it protects Fe-S proteins from oxidative stress and destruction of  
453 clusters. Such a hypothesis will need further investigation.

454 We assumed a function of GRXS17 in connection with its redox properties and  
455 hypothesized that it participates in signalling pathways related to the changes in the cellular  
456 redox status occurring in response to environmental variations. Of note, AtGRXS17 has been  
457 recently reported as prone to H<sub>2</sub>O<sub>2</sub>-induced Cys sulfenation (Wasczak et al., 2014). Redox  
458 changes might affect the subcellular localization of AtGRXS17 or the set of interacting

459 partners through post-translational redox modifications. Concerning the first point, our  
460 experiments (GFP-fusion and cellular fractionation) show that GRXS17 is localized in both  
461 nucleus and cytosol (Fig. 2), and a former study indicated that high temperature induces  
462 GRXS17 translocation from cytosol to nucleus (Wu et al., 2012). Thus, in response to  
463 environmental signals or to a specific physiological state, the GRXS17 function might be  
464 associated with nucleo-cytosolic shuttling. With regard to the 14 putative GRXS17 interaction  
465 partners identified by affinity chromatography, their localization is consistent with an  
466 interaction *in vivo*. Note that BOLA2, a possible transcriptional regulator interacting with  
467 GRXS17 in binary yeast two-hybrid and BiFC experiments (Couturier et al., 2014), was not  
468 isolated. This could originate from a low abundance or from the type of plant material used in  
469 this work. Nevertheless, the data gained from affinity experiments clearly show the ability of  
470 GRXS17 to interact with different types of partners, and thus to possibly modify their  
471 conformation or regulate their activity through post-translational redox modification.

472

#### 473 **GRXS17: a hub integrating hormonal and redox signals?**

474 Consistent with the pleiotropic phenotype of *grxS17* plants, Western data revealed the  
475 presence of the GRXS17 protein in all organs, particularly those containing actively dividing  
476 or elongating cells. In addition, *in situ* hybridization showed a high transcript level in apical  
477 meristem and histological analyses of plants grown in long day specifically revealed a larger  
478 cell size in both meristems and leaves of *grxS17* plants. All these data suggest a crucial role of  
479 GRXS17 in meristem activity and cell division. Several studies provided evidence for a tight  
480 relationship between intracellular redox status, disulfide reductases, and development  
481 (Considine and Foyer, 2014). For instance, the development of root meristems is influenced  
482 by changes in the overall redox status and auxin content/distribution (Vernoux et al., 2000;  
483 Jiang et al., 2003; Yu et al., 2013). Another example is the *A. thaliana ntra ntrb cad2* triple  
484 mutant, which is defective in TRX reduction and GSH synthesis, and exhibits strongly  
485 impaired reproductive development in relation to altered auxin metabolism (Bashandy et al.,  
486 2010). The plastidial TRXm3 is essential for meristem maintenance in Arabidopsis through a  
487 role in symplastic permeability (Benitez-Alfonso et al., 2009) and the nucleoredoxin NRX1  
488 participates in the establishment of pollen fertility (Qin et al., 2009; Marchal et al., 2014).  
489 With regard to GRXs, the fate of germ cells in maize anthers is determined by the redox status  
490 via a GRX, termed MSCA1, presumed to play a role in gene transcription (Kelliher and  
491 Walbot, 2012). The nuclear class-III GRXs, ROXY1 and 2, are required for proper

492 development of floral organs in *Arabidopsis* likely through interaction with TGA transcription  
493 factors (Xing and Zachgo, 2008; Hong et al., 2012). Altogether, these reports support the view  
494 that disulfide reductases finely control plant development.

495 *Arabidopsis grxS17* plants display hypersensitivity to high temperature and altered auxin-  
496 mediated signalling pathways in roots (Cheng et al., 2011). The present work unveils another  
497 function for GRXS17 in integrating photoperiod signals for proper development. Temperature  
498 is however an important determinant, since the phenotype is evident in long-day conditions at  
499 22°C and 28°C, but not at 15°C. In this study, we mainly investigated the phenotype of aerial  
500 parts of plants grown on soil and observed an altered shape of the leaves, which turned thick  
501 and elongated and displayed a reduced number of large cells. Looking for mutants with a  
502 similar phenotype (Bensmihen et al., 2008), we noticed that *drl1* and *elo* mutants exhibit  
503 elongated leaves and a strongly reduced number of larger palisade cells compared to WT  
504 (Nelissen et al., 2003; 2005). DRL1 regulates RNA polymerase II-mediated transcription  
505 through the elongator complex, which is composed of several ELO proteins and displays  
506 histone acetyltransferase activity preferentially in regions of auxin-related genes (Nelissen et  
507 al., 2010). Importantly, the floral development of *drl1* plants is delayed and the root  
508 development of both *elo* and *drl1* mutants is substantially reduced (Nelissen et al., 2003).  
509 Interestingly, by investigating the genes co-expressed with *GRXS17* using Genevestigator  
510 (Hruz et al., 2008), a high correlation was found with *ELO2* (At5g13680). It is thus tempting  
511 to hypothesize that the *grxS17* phenotype is linked to defects in ELO- and/or DRL1-  
512 dependent transcription mechanisms.

513

514 **Possible roles of GRXS17 in interaction with the NF-YC11/NC2 $\alpha$  nuclear factor**

515           Among the GRXS17 partners identified using affinity chromatography, we focused on  
516 the nuclear factor NF-YC11/NC2 $\alpha$ . Because the interaction between this factor and the GRX  
517 was confirmed by BiFC experiments in Arabidopsis protoplasts, a physiologically relevant  
518 interaction can be assumed. The *A. thaliana* NF-Y family comprises three main types (A, B

519 and C). Initially named CCAAT-binding factor or Heme Activator Protein (HAP), they  
520 usually form trimeric complexes of A, B and C subunits, binding to CCAAT-promoter  
521 sequences and transcriptionally regulating genes participating in plant development and stress  
522 responses (Dolfini et al., 2012; Laloum et al., 2013). In animal cells, they are central to cell

Figure 10

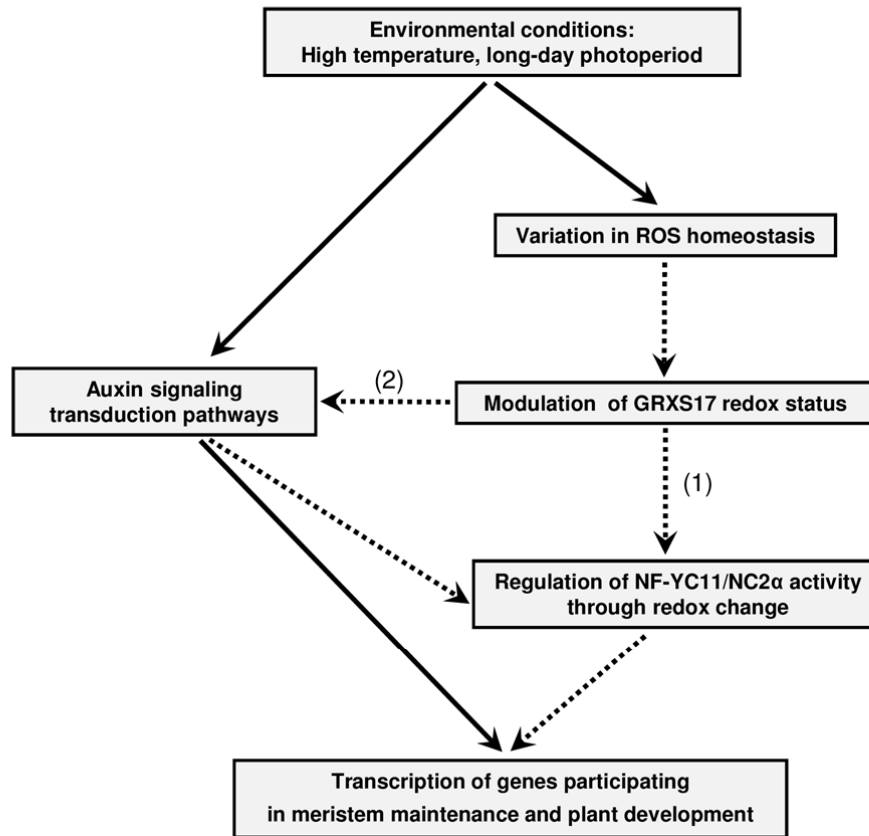


**Figure 10. Suggested role of GRXS17 during plant development in connection with environmental conditions and auxin-related mechanisms.**

Dotted lines indicate the proposed steps in signal transduction involving GRXS17. The model is based on the data presented in this work (1) and those reported in Cheng et al. (2011) (2).

523 cycle progression (Benatti et al., 2011) and in fungi, the corresponding trimeric complex  
524 formed by HAP2, 3 and 5 includes a fourth HAP4 subunit. Interestingly, in *S. pombe*, the  
525 function and subcellular localization of HAP4, which participates in iron homeostasis, is  
526 under the control of the multidomain GRX4 (Mercier and Labbé, 2009). In relation to the

527 *grxS17* phenotype, it is worth mentioning that AtNF-YC11 specifically interacts with AtNF-  
528 YB3, an isoform controlling flowering time (Kumimoto et al., 2008). To date, the only  
529 evidence for redox control was obtained for a mammalian NF-YB whose association to NF-  
530 YC is dependent on the reduction of an intermolecular disulfide bond (Nakshatri et al., 1996).  
531 Interestingly, all plant NF-YC11 orthologs exhibit a unique N-terminal sequence clearly  
532 distinguishing them from other NF-YCs. On this basis, they have been reclassified as  
533 homologs to NC2 $\alpha$  factors (Petroni et al., 2012). NC2 $\alpha$ , together with another factor called  
534 NC2 $\beta$ , forms a tight heterodimer able to associate with the TATA-binding complex and acts  
535 as a transcription repressor as shown in *S. cerevisiae* and rice (Kim et al., 1997; Song et al.,  
536 2002). Two cysteine residues are present in the NF-YC11/NC2 $\alpha$  N-terminal extension (Fig.  
537 S12). Of note, one is strictly conserved in plant orthologues and also in human NC2 $\alpha$  protein,  
538 while the position of the second varies in Dicotyledons and in Monocotyledons.  
539 Unfortunately, all attempts to produce recombinant NF-YC11/NC2 $\alpha$  failed which precluded  
540 investigations on a possible redox-mediated interaction with GRXS17. The data gained from  
541 the characterization of the Arabidopsis *nf-yc11/nc2 $\alpha$*  mutant line (Fig. 9; Fig. S11) revealed  
542 that the nuclear factor is a central element for proper plant development. In short-day  
543 conditions, *nf-yc11/nc2 $\alpha$*  plants display developmental defects (slow growth and altered floral  
544 spikes). Most interestingly, when comparing the phenotypes of *grxS17* and *nf-yc11/nc2 $\alpha$*   
545 plants, we noticed that both mutants share common photoperiod-dependent characteristics  
546 such as delayed appearance of the first two leaves, abnormal leaf shapes and impaired  
547 flowering (Fig. 9; Fig. S11). This phenotype resemblance, which is revealed in long day but  
548 not in short-day conditions, gives further credence to a concerted action of GRXS17 and NF-  
549 YC11/NC2 $\alpha$  in the control of plant development in relation to environmental conditions. We  
550 might thus speculate that GRXS17 modulates the NF-YC11/NC2 $\alpha$  function by controlling its  
551 redox state, and we propose a working model illustrating such a role for GRXS17 (Fig. 10).  
552 Based on the resemblance of *grxS17* and *nf-yc11/nc2 $\alpha$*  mutants, it is conceivable that  
553 GRXS17-mediated redox changes modify the capacity of AtNF-YC11/NC2 $\alpha$  to bind to a  
554 NC2 $\beta$  subunit (AtNF-YB11-13), ultimately resulting in the modification of the transcription  
555 level of genes involved in meristem maintenance and plant developmental programmes, such  
556 as those related to auxin action (Fig. 10). Taken collectively, these data lead us to propose that  
557 *A. thaliana* GRXS17 relays environmental signals, possibly via subtle changes in the  
558 cellular/nuclear redox state, and then enters this information into the control of gene  
559 transcription to initiate essential developmental steps. The use of mutant lines expressing

560 mutated GRXS17 and NF-YC11/NC2 $\alpha$  forms will help to determine the precise mechanisms  
561 underlying the functions of these two key actors in plant development in relation with the  
562 presence and the redox status of their cysteines.

563

## 564 **Material and Methods**

### 565 **Plant material and growth conditions**

566 *Arabidopsis thaliana* Col-0 plants were grown in standard conditions under an 8-h  
567 photoperiod and a photon flux density of 200  $\mu\text{mol photons m}^{-2} \text{s}^{-1}$  at 22°C. Other conditions  
568 of light (500  $\mu\text{mol photons m}^{-2} \text{s}^{-1}$ ), temperature (15°C or 28°C) and photoperiod (16 h or  
569 continuous light) were applied in controlled growth chambers either from sowing or on 2- to  
570 3-week old plants grown under standard conditions.

571

### 572 **Transformation of *A. thaliana* plants**

573 The full-length GRXS17 cDNA (At4g04950) was cloned into the pB2GW7 vector  
574 (GATEWAY, Invitrogen). Following transformation using *Agrobacterium tumefaciens* C58  
575 strain (Clough and Bent, 1998), homozygous lines (T2) were obtained from resistance  
576 segregation assays. Leaf genomic DNA was extracted using the DNeasy Plant Mini Kit  
577 (Qiagen) to perform PCR using appropriate primers (Table SIII), Taq DNA polymerase (Life  
578 Technologies) and the GeneAmp PCRSystem 2700 (Applied Biosystems). RT-PCR was  
579 performed using Sensiscript III (Life Technologies) following leaf RNA extraction  
580 (NucleoSpin, Macherey-Nagel).

581

### 582 **Expression of recombinant WT and Cys-mutant GRXS17**

583 AtGRXS17 cDNA was cloned into the pET-16b vector (Novagen, Merck Biosciences) for  
584 expression in *E. coli* BL21(DE3)-pLysS. The protein was purified by nickel-chelate  
585 chromatography (GE Healthcare). Site-directed mutagenesis was performed using the  
586 QuikChange II protocol (Stratagene) and appropriate primers (Table SIII).

587

### 588 ***In vitro* reconstitution assay of Fe-S clusters and analytical measurements**

589 GRXS17 (50  $\mu\text{M}$ ) was reconstituted *in vitro* by incubation with  $\text{Fe}(\text{NH}_4)_2(\text{SO}_4)_2$ , cysteine,  
590 GSH, pyridoxal phosphate, and *E. coli* IscS in the molar ratio of 1 GRX:6:9:10:0.04:0.02 in  
591 50 mM sodium phosphate buffer pH 8.0, 300 mM NaCl, 5 mM DTT under argon atmosphere  
592 for 2 h. After centrifugation (4 min, 4°C, 13,000 rpm), UV/visible spectra were recorded with

593 a Shimadzu UV-2100 spectrophotometer. Iron content was determined after reconstitution of  
594 100  $\mu$ M GRXS17 according to Fish (1988).

595

### 596 **Cytology and *in situ* hybridization**

597 Meristem cross sections were prepared using a microtome (Leica RM2255) from tissues fixed  
598 with formaldehyde/glutaraldehyde and embedded in hydroxyethyl methacrylate (Technovit  
599 7100; Heraeus Kulzer) and counterstained with Toluidine blue. Measurements of mesophyll  
600 cells were performed after propidium iodide (PI) staining (5 ng.mL<sup>-1</sup>). Confocal microscopic  
601 observations were carried out using the Axio observer Z1 microscope with the LSM 700  
602 scanning module, the ZEN 2010 software (Zeiss), and the PI (BP 566–1000) filters. *In situ*  
603 hybridization was performed as in Bashandy et al. (2010). After fixation, dehydration and  
604 embedding in paraffin wax, sample sections (7- $\mu$ m thick) were attached to precoated glass  
605 slides (DAKO). Probes were synthesized using digoxigenin (DIG)-UTP (Boehringer  
606 Mannheim). Immunodetection was performed using an anti-DIG antibody coupled to alkaline  
607 phosphatase.

608

### 609 **Transient transformation of protoplasts with GFP and split-YFP constructs**

610 Protoplasts were isolated from leaves of 6-week-old *A. thaliana* plants for transient expression  
611 of fusion proteins (Wojtera-Kwiczor et al., 2013). cDNAs encoding GRXS17 and NF-  
612 YC11/NC2 $\alpha$  were cloned in sense direction into the pGFP2-vector for C-terminal GFP fusion.  
613 The GRXS17 and NF-YC11/NC2 $\alpha$  cDNAs were inserted in frame with YFP N- and C-  
614 terminal parts in pSPYNE and pSPYCE vectors obtained from Jörg Kudla (University of  
615 Muenster). Combinations of empty vectors and fusion constructs were used as controls. GFP  
616 and chlorophyll autofluorescence were visualized with excitation at 488 nm and emission at  
617 500-530 nm and 650-710 nm, respectively, using the cLSM 510 META (Carl Zeiss). YFP  
618 was visualized with excitation at 514 nm and emission at 535-590 nm.

619

### 620 **Affinity chromatography and electrospray ionization (ESI) mass spectrometry**

621 His-tagged GRXS17 was bound to a Ni-NTA-column and used as affinity matrix. Leaves of  
622 5-week old plants grown under short-day conditions were homogenized in 20 ml 50 mM  
623 Bicine, pH 7.8, 100 mM sucrose, 50 mM NaCl. After filtration through Miracloth and  
624 centrifugation (10 min, 6,000  $xg$ , 4°C and 50 min, 4°C, 100,000  $xg$ ), the clarified supernatant  
625 (30 mg protein) was applied to the matrix and incubated for 2 h at 4°C. Non-bound material

626 was removed by washing the column 4 times with 10 ml 20 mM Bicine, pH 7.8. Elution was  
627 achieved with 4 ml of the same buffer containing 150 mM DTT. After tryptic digestion (50  
628 µg proteins per analysis), the fragments were separated by reverse-phase HPLC and analyzed  
629 by ESI-MS (Holtgreffe et al., 2008). Results were analyzed using the Bruker Daltronics  
630 software.

631

### 632 **Biochemical methods**

633 Plant soluble proteins were prepared, separated by SDS-PAGE and electro-transferred onto a  
634 nitrocellulose membrane (Pall Corporation) (Rey et al., 2005). Protein crosslinking was  
635 achieved using dimethyl pimelimidate/2 HCl (DMP) (Thermo Fisher Scientific) (Riondet et  
636 al., 2012). Polyclonal antibodies were raised in rabbit against His-tagged AtGRXS17  
637 (Genecust). Immunodetection of AtGRXS17 was carried out using primary antibodies diluted  
638 1:1000 and the goat anti-rabbit “Alexa Fluor® 680” IgG (1:10,000) (Invitrogen). Bound  
639 antibodies were revealed at 680 nm using the Odyssey Infrared Imager (LiCor). For  
640 immunodetection of aconitase (Bernard et al., 2009) and PsaA (Agrisera), horse-radish  
641 peroxidase-conjugated secondary antibodies and chemiluminescence were used.  
642 Autoluminescence imaging of lipid peroxidation was performed as in Collin et al. (2008).

643

### 644 **Yeast plasmids, strains and growth conditions**

645 The GRXS17 entire sequence and each GRX module, M2 (S17<sub>167-252</sub>), M3 (S17<sub>297-383</sub>) and  
646 M4 (S17<sub>404-488</sub>) were cloned in-frame in the yeast plasmid pMM221. pMM221 contains the  
647 *S. cerevisiae* GRX5 mitochondrial targeting sequence plus a C-terminal 3HA/His6 tag, under  
648 the control of the doxycycline-regulatory tetO2 promoter (Tables SI and SIII) (Molina et al.,  
649 2004). pMM54 contains a yeast *GRX5*-3HA construction under its endogenous promoter  
650 (Rodriguez-Manzaneque et al., 2002). Strains are described in Table SII. Plasmids were  
651 linearized by *Clal* previous to chromosomal integration. Samples were taken from cultures  
652 grown exponentially (Molina et al., 2004) for at least 10 generations at 30°C. Sensitivity to  
653 oxidants was determined on YPD plates, by spotting 1:5 serial dilutions of exponential  
654 cultures and recording growth after 2 days at 30°C. Subfractionation of mitochondria was  
655 performed as in Bandyopadhyay et al. (2008). Northern blot analyses using yeast RNA were  
656 performed with digoxigenin (Belli et al., 1998). Gene probes were generated by PCR from  
657 genomic DNA using appropriate oligonucleotides (Table SIII).

658

659 **Enzyme activity determinations**

660 Aconitase and malate dehydrogenase were assayed in extracts from yeast growing  
661 exponentially in YPGalactose medium (Robinson et al., 1987). Isopropylmalate isomerase  
662 activity was determined in extracts prepared from cells growing exponentially in SC medium  
663 supplemented with the specific auxotrophy requirement (Pierik et al., 2009). In the case of  
664 leucine, only 1/3 of the standard concentration was added into the medium to allow growth.  
665 In-gel activity assays for aldehyde oxidase and aconitase were as previously described  
666 (Bernard et al., 2009).

667

668 **Acknowledgements**

669 We are very grateful to the Groupe de Recherche Appliquée en Phytotechnologie (CEA,  
670 IBEB, SBVME) for technical assistance with controlled growth chambers, P. Henri for  
671 valuable technical assistance, D. Cerveau, B. Ksas and Dr. M. Havaux for helpful assistance  
672 in phenotype characterization and imaging experiments. We also wish to thank Drs. M.  
673 Bendahmane and M. Vandenbussche (Laboratoire de Reproduction et Développement des  
674 Plantes - UMR 5667 ENS-CNRS-INRA-Université de Lyon) for fruitful discussion about NF-  
675 Y transcription factors.

676

677 **Figure legends**

678 **Figure 1. Expression of *GRXS17* in *A. thaliana* plants.**

679 (A-B) Western analysis of *GRXS17* abundance. (A) Western blot analysis in flowers from WT  
680 and *grxS17* plants, and in organs of WT plants grown under standard conditions (20 µg per  
681 lane). The RubisCO large subunit (LSU) appears as a light grey background band in the  
682 *grxS17* lane. R, root from adult plant; S, stem from bolting plant; YL, young leaf; ML, mature  
683 leaf; OL, old leaf; B, floral bud; F, flower. (B) Loading controls: Coomassie blue stained gels  
684 (50-kDa region). (C-F) RNA *in situ* hybridization. Longitudinal sections of WT meristem  
685 inflorescences (C, D) and flower buds (E, F). Hybridizations were performed with antisense  
686 (C, E) or sense (D, F) *GRXS17* cDNA probes.

687

688 **Figure 2. Subcellular localization and dimerisation of *GRXS17*.**

689 (A) Transient expression of a *GRXS17*:GFP fusion in *A. thaliana* mesophyll protoplasts.  
690 Autofluorescence of chlorophyll indicates chloroplasts. (B) Stable expression of a  
691 *GRXS17*:GFP fusion in *Arabidopsis thaliana* leaves. White arrows indicate nuclei. (C)

692 Immunodetection of GRXS17, thioredoxin TRXh5 and nucleolin NUC1 in cytosolic (Cyt)  
693 and nuclear (Nuc) extracts of *Arabidopsis* flower buds. (D) Bimolecular fluorescence  
694 complementation assay of GRXS17. Vectors encoding C- and N-terminal split-YFP fusions  
695 with GRXS17 were co-transformed into *Arabidopsis thaliana* mesophyll protoplasts. (E)  
696 Immunodetection of GRXS17 in *grxS17* and WT extracts cross-linked (C) or not (NC) with  
697 DMP.

698

699 **Figure 3. Growth and development of plants modified in *GRXS17* expression as a**  
700 **function of photoperiod and temperature.**

701 (A) Five-week old plants grown in standard conditions (8-h photoperiod, 200  $\mu\text{mol photons}$   
702  $\text{m}^{-2} \text{s}^{-1}$ ) at 22°C. (B) Plants grown for 2.5 weeks in standard conditions and transferred to 28°C  
703 (8-h photoperiod, 200  $\mu\text{mol photons m}^{-2} \text{s}^{-1}$ ) for 2.5 weeks. The arrow indicates the absence of  
704 young leaves. (C) Plants grown in long-day photoperiod conditions (16 h, 200  $\mu\text{mol photons}$   
705  $\text{m}^{-2} \text{s}^{-1}$ ) at 22°C. (D) Plants grown for 2 weeks in standard conditions and transferred to  
706 continuous light (200  $\mu\text{mol photons m}^{-2} \text{s}^{-1}$ , 22°C) for 3 weeks. (E) Plants grown for 2 weeks  
707 in standard conditions and transferred to 28°C and long-day photoperiod (16 h, 200  $\mu\text{mol}$   
708  $\text{photons m}^{-2} \text{s}^{-1}$ ) for 2.5 weeks. (F) Plants grown for 3 weeks in standard conditions and  
709 transferred to 15°C and long-day photoperiod (16 h, 200  $\mu\text{mol photons m}^{-2} \text{s}^{-1}$ ) for 4 weeks.  
710 WT, Wild-type plants; *grxS17*, homozygous SALK\_021301 plants; *grxS17 GRXS17* 3.3 and  
711 17.8, two independent *grxS17* lines expressing *GRXS17*. SD and LD, short (8 h) and long (16  
712 h) day.

713

714 **Figure 4. Structure of shoot apical meristem (SAM) and leaves in *grxS17* plants.**

715 (A) Histological structure of the SAM stained by toluidine blue in 7-day old wild-type,  
716 *grxS17* and *grxS17 GRXS17* (line 3.3) plants grown in long-day conditions (16 h) and high  
717 light (500  $\mu\text{mol photons m}^{-2} \text{s}^{-1}$ ). (B) Observation of mesophyll cells in leaves of 3-week old  
718 plants grown under long-day/high-light conditions. (C) Number of L1, L2 and L3 layer stem  
719 cells in SAM cross-sections shown in (A). Ten sections per genotype were analyzed. (D)  
720 Density of mesophyll cells in the sections shown in (B) (n: 12). \*, value significantly different  
721 from Wt value with  $p < 0.05$  (t-test).

722

723 **Figure 5. Incorporation of Fe-S clusters into recombinant WT and mutated AtGRXS17.**

724 (A) Domain structure of GRXS17. TRX-HD: TRX-like homology domain; M2-GRX, M3-  
725 GRX and M4-GRX: three monothiol-GRX domains. Positions of active-site cysteines are  
726 indicated by black triangles and that of other cysteine by a grey triangle. (B) Absorption  
727 spectra of GRXS17 and cysteine mutants. UV-visible absorption spectra were recorded  
728 immediately after *in vitro* reconstitution in anaerobic conditions. The active-site cysteines of  
729 each GRX domain were individually or together substituted by serines (M2:C179S; M3:  
730 C309S; M4: C416S; C179/309/416S). (C) Relative absorption at 420 nm of GRXS17  
731 mutants.

732

733 **Figure 6. Rescue of the *S. cerevisiae grx5* mutant defects by AtGRXS17.**

734 (A) Sensitivity to *t*-BOOH or diamide. The indicated yeast strains were spotted on YPD plates  
735 at 10x serial dilutions and grown for 3 days at 30°C on YPD plates. (B) Growth on glucose  
736 (YPD plates) or glycerol (YPGly plates) after 3 days at 30°C. (C) Relative ratio between  
737 aconitase and malate dehydrogenase activities, normalized with respect to the ratio in the WT  
738 strain, in exponential cultures at 30°C in YPGalactose medium. (D) Relative specific Leu1  
739 activity. (E) Northern blot analysis of *FIT3* and *FTR1* mRNA levels from exponential cultures  
740 at 30°C. Loading control: *SNR19* mRNA. (F) Relative iron content from exponential cultures  
741 at 30°C in YPD medium. Mean  $\pm$  SD (n = 3). Asterisks indicate statistically significant  
742 differences (Student's *t*-test,  $p < 0.05$ ) compared to WT (*GRX5*) cultures.

743

744 **Figure 7. Activities and levels of Fe-S enzymes in plants modified in *GRXS17* expression.**

745 Wild type (WT), a *grxS17* knock-out mutant and two complemented lines (3.3 and 17.8) were  
746 grown for 14 days under standard conditions (22°C) or transferred to 28°C after 7 days (Fig.  
747 S10). Mutant alleles in the *ABC Transporter of the Mitochondria 3* (*atm3-1* and *atm3-4*) were  
748 used for comparison. (A) Activities of aconitase (ACO) and aldehyde oxidase (AO) isozymes  
749 visualized as a formazan precipitate in a native gel assay. Cytosolic (cyto) and mitochondrial  
750 (mito) isoforms of ACO are indicated. Equal protein amounts (160  $\mu$ g for ACO and 60  $\mu$ g for  
751 AO) were loaded per lane. Immunoblotting of ACO and PsaA (a subunit of PSI) in  
752 Arabidopsis seedlings (10  $\mu$ g protein per lane) and loading control (Ponceau). (B) Relative  
753 activities of cytosolic and mitochondrial aconitase isoforms quantified using ImageJ software.  
754 The values are given as percentages of the sum of the band intensities per lane (mean  $\pm$  SD).  
755 The data are representative of 3 independent experiments.

756

757 **Figure 8. Localisation of NF-YC11/NC2 $\alpha$  and interaction with GRXS17.**

758 Isolated *A. thaliana* mesophyll protoplasts were transiently transformed with a NF-  
759 YC11/NC2 $\alpha$ :GFP fusion (A) or with split-YFP constructs containing GRXS17 or NF-  
760 YC11/NC2 $\alpha$  (B). White arrows indicate nuclei.

761

762 **Figure 9. Characterization of a *nf-yc11/nc2 $\alpha$*  mutant and comparison of the growth of**  
763 ***grxS17* and *nf-yc11/nc2 $\alpha$*  plants as a function of photoperiod duration.**

764 (A) PCR analysis of genomic DNA of At3g12480 and T-DNA in WT, heterozygous (Htz) and  
765 homozygous (Hmz) plants of the GABI-042E02 mutant line. (B) RT-PCR analysis of WT and  
766 homozygous plants. (C) Seedling development in short- and long-day conditions (8- and 16-h,  
767 respectively) at moderate light (200  $\mu\text{mol photons m}^{-2} \text{s}^{-1}$ ) and 22°C. The seedlings were  
768 grown simultaneously in the same conditions and the original photographs are shown in Fig.  
769 S 10. (D) Vegetative growth of plants in standard light conditions (short-day: 8-h photoperiod  
770 and moderate light, 200  $\mu\text{mol photons m}^{-2} \text{s}^{-1}$ ) and in long-day and high-light conditions (16-h  
771 photoperiod, 500  $\mu\text{mol photons m}^{-2} \text{s}^{-1}$ ) at 22°C. The plant age is indicated for each genotype  
772 and culture condition. Scale bars: 1 and 6 cm in C and D, respectively.

773

774 **Figure 10. Suggested role of GRXS17 during plant development in connection with**  
775 **environmental conditions and auxin-related mechanisms.**

776 Dotted lines indicate the proposed steps in signal transduction involving GRXS17. The model  
777 is based on the data presented in this work (1) and those reported in Cheng et al. (2011) (2).

778

779

780 **Table I. Putative interaction partners of AtGRXS17.** The list includes the proteins  
 781 identified at least 4 times in 15 independent affinity chromatography experiments with His-  
 782 tagged AtGRXS17.

Accession number	Protein name	Function	Subcellular localization <sup>a</sup>	Sequence length (aa)	Protein identification (times) <sup>b</sup>	Sequence coverage (%) <sup>c</sup>
At4g04950	GRXS17	Cell redox homeostasis	CY,NU,PL	488	15	90%
At1g50570	Calcium-dependent lipid-binding family protein	Unknown	NU	388	13	68%
At3g12480	NF-YC11/NC2 $\alpha$	Transcription factor	CY,MI,NU,PL	293	7	59%
At4g25860	Oxysterol-binding protein-related protein 4A	Sterol transport	CY	386	11	56%
At3g13460	CIPK1 interacting protein ECT2	Unknown	CY,NU,PL	667	6	52%
At2g39960	Microsomal signal peptidase	Peptidase activity	CY,ER,MI,PM	192	5	45%
At1g13440	GapC2	Glycolysis	CY,MI,NU,PL,PX	338	9	41%
At5g46570	BR-signaling kinase 2	Protein phosphorylation	CY,PM	492	5	41%
At4g31180	Aspartate-tRNA ligase-like protein	Aspartyl-tRNA synthetase activity	CY,PL	270	4	31%
At5g11870	Alkaline phytoceramidase	Hydrolase activity	ES,MI,PL,PM	270	8	28%
At5g54050	Cysteine/histidine-rich C1 domain-containing protein	Protein-disulfide reductase activity	ES, NU	580	8	21%
At5g20830	Sucrose synthase 1	UDP-glycosyltransferase activity	CY,MI	808	4	19%
At1g24510	T-complex protein 1 subunit epsilon	Chaperone activity	CY,MI,PM	535	6	18%
At4g22030	Probable F-box protein	Unknown	CY,MI,PL	626	5	12%

<sup>a</sup>Sub-cellular localization predicted by BAR Cell eFP Browser. CY: Cytosol; ER: Endoplasmic reticulum; ES: Extracellular space; MI: Mitochondria; NU: Nucleus; PX: Peroxisome; PM: Plasma membrane; PL: Plastid

<sup>b</sup>Proteins were identified due to the presence of their peptides in the indicated number of experiments.

<sup>c</sup>Identified peptides with a MOWSE score greater 15 were used to calculate the total sequence coverage.

783

784

785

786

787

788 **Supplemental data**

789 **Table SI. Plasmids employed for experiments on yeast.**

790

791 **Table SII. Yeast strains.**

792

793 **Table SIII. List of primers employed in the study.**

794

795 **Figure S1. Molecular characterization of *A. thaliana* plants modified in *GRXS17***  
796 **expression and *GRXS17* protein abundance.**

797 (A) PCR analysis of *GRXS17* gene and *GRXS17* cDNA in the genomic DNA of WT plants,  
798 of SALK\_021301 T-DNA homozygous plants (*grxS17*) and of two independent lines of T-  
799 DNA plants expressing the *GRXS17* cDNA under the control of the cauliflower mosaic virus  
800 35S promoter (*grxS17 GRXS17* 3.3 and 17.8). (B) Western blot analysis of *GRXS17*  
801 abundance in leaf soluble proteins (20 µg per lane). The grey band in *grxS17* lane is attributed  
802 to a non-specific signal from the large RubisCO subunit which has almost the same size as  
803 *GRXS17*.

804

805 **Figure S2. Subcellular localization of *GRXS17*.**

806 Immunodetection of *GRXS17*, nuclear histone H3, cytosolic thioredoxin h3 (TRXh3),  
807 mitochondrial thioredoxin o1 (TRXo1) and plastidial 2-Cys peroxiredoxin (2-Cys PRX) in  
808 nuclear (Nuc), cytosolic (Cyt), mitochondrial (Mit) and chloroplastic (Chl) fractions prepared  
809 from Arabidopsis plants. The faint histone H3 band detected in mitochondrial fraction  
810 probably indicates a slight contamination from nuclei.

811

812 **Figure S3. Controls of the bimolecular fluorescence complementation assay of *GRXS17***  
813 **and NF-YC11/NC2α.**

814 Vectors encoding C- and N-terminal split-YFP fusions with *GRXS17* or NF-YC11/NC2α and  
815 empty vectors were co-transformed into *A. thaliana* mesophyll protoplasts. Pictures were  
816 taken 14 h after transformation.

817

818

819

820 **Figure S4. Growth and development of *A. thaliana* plants modified in *GRXS17***  
821 **expression as a function of light and temperature regimes.**

822 (A) Five-week old plants grown for 2 weeks in standard conditions and then transferred for 3  
823 weeks to high-light ( $500 \mu\text{mol photons m}^{-2} \text{s}^{-1}$ ) and short-day (8-h photoperiod) conditions at  
824  $22^\circ\text{C}$ . (B) Three-week old plants grown in high-light ( $500 \mu\text{mol photons m}^{-2} \text{s}^{-1}$ ) and long-day  
825 (16-h photoperiod) conditions at  $22^\circ\text{C}$ . (C) Seven-week old plants grown for 3 weeks in  
826 standard conditions and then transferred to  $15^\circ\text{C}$ , long-day photoperiod (16 h) and high-light  
827 conditions ( $500 \mu\text{mol photons m}^{-2} \text{s}^{-1}$ ) for 4 weeks. WT, wild-type plants; *grxS17*,  
828 homozygous SALK\_021301 plants; *grxS17 GRXS17* 3.3 and 17.8, two independent KO lines  
829 expressing *GRXS17*.

830

831 **Figure S5. Floral development of *A. thaliana* plants modified in *GRXS17* expression as a**  
832 **function of photoperiod and light intensity.**

833 (A) 54-day old plants grown in standard conditions (8-h photoperiod,  $200 \mu\text{mol photons m}^{-2}$   
834  $\text{s}^{-1}$  at  $22^\circ\text{C}$ ). (B) Four-week old plants grown in high-light ( $500 \mu\text{mol photons m}^{-2} \text{s}^{-1}$ ) and  
835 long-day (16-h photoperiod) conditions at  $22^\circ\text{C}$ . (C) and (D) Height of the main floral spike  
836 in plants grown in standard conditions for 54 days and in high-light and long-photoperiod  
837 conditions for 4 weeks, respectively. (E) and (F) Number of leaves at flowering in plants  
838 grown in standard conditions and in high-light and long-day conditions, respectively. (G)  
839 Five-week old *grxS17* plant grown in high-light ( $500 \mu\text{mol photons.m}^{-2}.\text{s}^{-1}$ ) and long-day (16-  
840 h photoperiod) conditions at  $22^\circ\text{C}$ . WT, Wild-type plants; *grxS17*, homozygous  
841 SALK\_021301 plants; *grxS17 GRXS17* 3.3 and 17.8, two independent KO lines expressing  
842 *GRXS17*. \*\*\*, significantly different from the WT value with  $p < 0.01$  (t test).

843

844 **Figure S6. Autoluminescence in *A. thaliana* plants modified in *GRXS17* expression.**

845 (A) Three-week old plants grown in high-light ( $500 \mu\text{mol photons m}^{-2} \text{s}^{-1}$ ) and long-day (16-h  
846 photoperiod) conditions at  $22^\circ\text{C}$ . (B) Autoluminescence imaging of lipid peroxidation in these  
847 plants. The homogeneous blue/purple color of plants indicates the absence of photodamage  
848 (compare panel D for positive control). WT, wild-type plants; *grxS17*, homozygous  
849 SALK\_021301 plants; *grxS17 GRXS17* 3.3 and 17.8, two independent KO lines expressing  
850 *GRXS17*. (C) Five-week old WT plant grown in standard conditions (8-h photoperiod,  $200$   
851  $\mu\text{mol photons m}^{-2} \text{s}^{-1}$  at  $22^\circ\text{C}$ ) and then exposed to a photooxidative treatment for 1 day (8-h  
852 photoperiod,  $1250 \mu\text{mol photons m}^{-2} \text{s}^{-1}$  at  $6^\circ\text{C}$ ). The red arrows indicate leaves displaying

853 bleaching resulting from photodamage. (D) Autoluminescence imaging of lipid peroxidation  
854 in the plant shown in panel C. The damaged leaves appear in white/yellow color due to the  
855 photon emission associated with lipid peroxidation.

856

857 **Figure S7. Structure of the shoot apical meristem (SAM) in the *grxS17* mutant.**

858 (A) Histological structure of the SAM stained by toluidine blue in WT, *grxS17* and *grxS17*  
859 *GRXS17* (line 3.3) seedlings grown for 11 days in short-day (8 h) conditions and standard  
860 light (200  $\mu\text{mol photons m}^{-2} \text{s}^{-1}$ ). (B) Number of L1, L2 and L3 layer stem cells in cross-  
861 sections of SAM shown in (A). Ten sections per genotype were analyzed.

862

863 **Figure S8. Hypothetical structure of GRXS17 and amino acid alignment of the three**  
864 **GRX domains M2, M3 and M4 from *A. thaliana*.** The structures of the single domains were  
865 generated from 1XFL and 3L4N pdb entries for TRX and GRX proteins, respectively, and are  
866 not experimentally confirmed. The linker regions and the relative positions of the TRX  
867 domain are speculative.

868

869 **Figure S9. Analysis of the GRXS17 forms expressed in *S. cerevisiae*.**

870 (A) Western blot analysis with anti-HA antibodies (10  $\mu\text{g}$  total proteins from cell extracts per  
871 lane). Extracts from yeast cells expressing the homologous GRX5 protein under the native  
872 promoter (*Grx5 Sc*) are included as control. Samples from cells grown in fermentative  
873 conditions (*Glu*) and in respiratory conditions (*Lac*) were run in parallel. Molecular size of the  
874 expressed S17 forms is indicated. (B) Subfractionation of extracts from *S. cerevisiae* cells  
875 expressing the respective S17 forms and grown in respiratory conditions (lactose medium).  
876 TE (total extracts, 25  $\mu\text{g}$ ), MT (total mitochondria, 5  $\mu\text{g}$ ), IMS (intermembrane mitochondrial  
877 space, 5  $\mu\text{g}$ ), MX (mitochondrial matrix, 5  $\mu\text{g}$ ). Alpha-ketoglutarate dehydrogenase ( $\alpha$ -KDH)  
878 is shown as a control of a mitochondrial matrix protein.

879

880 **Figure S10. Growth phenotypes and quantification of aldehyde oxidase enzyme activity**  
881 **in plants modified in *GRXS17* expression.**

882 *GrxS17* knockout seedlings were grown under normal and heat stress conditions and  
883 compared to complemented lines (3.3 and 17.8) and wild type (WT). For comparison, a weak  
884 (*atm3-4*) and a strong mutant allele (*atm3-1*) of *ATM3* were analysed, which are known to  
885 have decreased activities of cytosolic Fe-S enzymes. Plants were grown in long photoperiod

886 (16 h) at 22°C for 14 days (white bars), or shifted to 28°C after 7 days (grey bars). (A) Images  
887 of *grxS17* mutants and controls grown under standard conditions and under heat stress. Scale  
888 bar = 1 cm. (B) Quantification of the band intensities in native gels (Fig. 7) reflecting the  
889 major aldehyde oxidase activity using ImageJ. Activities are shown as percentage of WT  
890 levels (mean  $\pm$  SD; n = 3).

891

892 **Figure S11. Development of *nf-yc11/nc2a* plants as a function of light environment.**

893 (A) Development of seedlings in short- and long-day conditions (8-h and 16-h, respectively)  
894 at moderate light (200  $\mu\text{mol photons m}^{-2} \text{s}^{-1}$ ) and 22°C. (B) Phenotype of plants grown in  
895 long-day (16 h photoperiod) and moderate light (200  $\mu\text{mol photons m}^{-2} \text{s}^{-1}$ ) conditions at  
896 22°C. (C) Reproductive development of *nf-yc11/nc2a* plants in short- or long-day conditions  
897 at moderate or high light (200 or 500  $\mu\text{mol photons m}^{-2} \text{s}^{-1}$ , respectively) and 22°C. Scale  
898 bars: 6 cm. The plant age and culture condition are indicated for each genotype.

899

900 **Figure S12. Sequence alignment of plant, human and yeast proteins containing a NC2 $\alpha$**   
901 **domain.**

902 Alignment was performed using the ClustalW software At, *Arabidopsis thaliana* (At3g12480,  
903 NP\_187854.2); Mt, *Medicago truncatula* (XP\_003628014.1); St, *Solanum tuberosum*  
904 (XP\_006347683.1); Pt, *Populus trichocarpa* (XP\_002304814.1); Vv, *Vitis vinifera*  
905 (CAN71308.1); Os, *Oryza sativa* (AF464904); Bd, *Brachypodium distachyon*  
906 (XP\_003577492.1); Zm, *Zea mays* (NP\_001105089.1); Hs, *Homo sapiens* (AAB02192.1); Sc,  
907 *Saccharomyces cerevisiae* (NP\_011086.3). Amino acids are given using standard single-letter  
908 designation, and dashes indicate gaps. Stars and colons indicate identity and similarity of  
909 amino acids, respectively. The cysteine conserved in plant and human proteins is highlighted  
910 in yellow, the cysteines conserved in dicotyledonous and monocotyledonous plants are  
911 highlighted in blue and green, respectively. The black line indicates the NC2 $\alpha$  domain.

912

913

## Parsed Citations

**Balk J, Schaedler TA (2014) Iron cofactor assembly in plants. *Annu Rev Plant Biol* 65: 125-153**

PubMed: <http://www.ncbi.nlm.nih.gov/pubmed/24498975?dopt=abstract>

CrossRef: <http://dx.doi.org/10.1146/annurev-arplant-050213-035759>

Google Scholar: [Author Only](#) [Title Only](#) [Author and Title](#)

**Bandyopadhyay S, Gama F, Molina-Navarro MM, Gualberto JM, Claxton R, Naik SG, Huynh BH, Herrero E, Jacquot JP, Johnson MK, Rouhier N (2008) Chloroplast monothiol glutaredoxins as scaffold proteins for the assembly and delivery of [2Fe-2S] clusters. *EMBO J* 27: 1122-1133**

PubMed: <http://www.ncbi.nlm.nih.gov/pubmed/18354500?dopt=abstract>

CrossRef: <http://dx.doi.org/10.1038/emboj.2008.50>

Google Scholar: [Author Only](#) [Title Only](#) [Author and Title](#)

**Bashandy T, Guillemot J, Vernoux T, Caparros-Ruiz D, Ljung K, Meyer Y, Reichheld JP (2010) Interplay between the NADP-linked thioredoxin and glutathione systems in Arabidopsis auxin signalling. *Plant Cell* 22: 376-391**

PubMed: <http://www.ncbi.nlm.nih.gov/pubmed/20164444?dopt=abstract>

CrossRef: <http://dx.doi.org/10.1105/tpc.109.071225>

Google Scholar: [Author Only](#) [Title Only](#) [Author and Title](#)

**Belli G, Gari E, Piedrafita L, Aldea M, Herrero E (1998) An activator/repressor dual system allows tight tetracycline-regulated gene expression in budding yeast. *Nucl Acids Res* 26: 942-947**

PubMed: <http://www.ncbi.nlm.nih.gov/pubmed/9461451?dopt=abstract>

CrossRef: <http://dx.doi.org/10.1093/nar/26.4.942>

Google Scholar: [Author Only](#) [Title Only](#) [Author and Title](#)

**Benatti P, Dolfini D, Viganò A, Ravo M, Weisz A, Imbriano C (2011) Specific inhibition of NF-Y subunits triggers different cell proliferation defects. *Nucl Acids Res* 39: 5356-5368**

PubMed: <http://www.ncbi.nlm.nih.gov/pubmed/21415014?dopt=abstract>

CrossRef: <http://dx.doi.org/10.1093/nar/gkr128>

Google Scholar: [Author Only](#) [Title Only](#) [Author and Title](#)

**Benitez-Afonso Y, Cilia M, San Roman A, Thomas C, Maule A, Hearn S, Jackson D (2009) Control of Arabidopsis meristem development by thioredoxin-dependent regulation of intercellular transport. *Proc Natl Acad Sci USA* 106: 3615-3620**

PubMed: <http://www.ncbi.nlm.nih.gov/pubmed/19218459?dopt=abstract>

CrossRef: <http://dx.doi.org/10.1073/pnas.0808717106>

Google Scholar: [Author Only](#) [Title Only](#) [Author and Title](#)

**Bensmihen S, Hanna AI, Langlade NB, Micol JL, Bangham A, Coen ES (2008) Mutational spaces for leaf shape and size. *HFSP J* 2: 110-120**

PubMed: <http://www.ncbi.nlm.nih.gov/pubmed/19404477?dopt=abstract>

CrossRef: <http://dx.doi.org/10.2976/1.2836738>

Google Scholar: [Author Only](#) [Title Only](#) [Author and Title](#)

**Bernard DG, Cheng Y, Zhao Y, Balk J (2009) An allelic mutant series of ATM3 reveals its key role in the biogenesis of cytosolic iron-sulfur proteins in Arabidopsis. *Plant Physiol* 151: 590-602**

PubMed: <http://www.ncbi.nlm.nih.gov/pubmed/19710232?dopt=abstract>

CrossRef: <http://dx.doi.org/10.1104/pp.109.143651>

Google Scholar: [Author Only](#) [Title Only](#) [Author and Title](#)

**Cheng NH (2008) AtGRX4, an Arabidopsis chloroplastic monothiol glutaredoxin, is able to suppress yeast grx5 mutant phenotypes and respond to oxidative stress. *FEBS Lett* 582: 848-854**

PubMed: <http://www.ncbi.nlm.nih.gov/pubmed/18275854?dopt=abstract>

Google Scholar: [Author Only](#) [Title Only](#) [Author and Title](#)

**Cheng NH, Liu JZ, Brock A, Nelson RS, Hirschi KD (2006) AtGRXcp, an Arabidopsis chloroplastic glutaredoxin, is critical for protection against protein oxidative damage. *J Biol Chem* 281: 26280-26288**

PubMed: <http://www.ncbi.nlm.nih.gov/pubmed/16829529?dopt=abstract>

CrossRef: <http://dx.doi.org/10.1074/jbc.M601354200>

Google Scholar: [Author Only](#) [Title Only](#) [Author and Title](#)

**Cheng NH, Liu JZ, Liu X, Wu Q, Thompson SM, Lin J, Chang J, Whitham SA, Park S, Cohen JD, Hirschi KD (2011) Arabidopsis monothiol glutaredoxin, AtGRXS17, is critical for temperature-dependent postembryonic growth and development via modulating auxin response. *J Biol Chem* 286: 20398-20406**

PubMed: <http://www.ncbi.nlm.nih.gov/pubmed/21515673?dopt=abstract>

Google Scholar: [Author Only](#) [Title Only](#) [Author and Title](#)

**Clough SJ, Bent AF (1998) Floral dip: a simplified method for Agrobacterium-mediated transformation of Arabidopsis thaliana. *Plant J* 16: 735-43**

PubMed: <http://www.ncbi.nlm.nih.gov/pubmed/10069079?dopt=abstract>

CrossRef: <http://dx.doi.org/10.1046/j.1365-313x.1998.00343.x>

Google Scholar: [Author Only](#) [Title Only](#) [Author and Title](#)

**Collin V, Eymery F, Genty B, Rey P, Havaux M (2008) Vitamin E plays a crucial role in the tolerance of Arabidopsis thaliana to oxidative stress induced by heavy metals. *Plant Cell Environ* 31: 244-257**

PubMed: <http://www.ncbi.nlm.nih.gov/pubmed/17996014?dopt=abstract>

Google Scholar: [Author Only](#) [Title Only](#) [Author and Title](#)

**Considine MJ, Foyer CH (2014) Redox regulation of plant development. *Antioxid Redox Signal* 21: 1305-1326**

PubMed: <http://www.ncbi.nlm.nih.gov/pubmed/24180689?dopt=abstract>  
CrossRef: <http://dx.doi.org/10.1089/ars.2013.5665>  
Google Scholar: [Author Only Title Only Author and Title](#)

**Couturier J, Jacquot JP, Rouhier N (2009) Evolution and diversity of glutaredoxins in photosynthetic organisms. Cell Mol Life Sci 66: 2539-2557**

PubMed: <http://www.ncbi.nlm.nih.gov/pubmed/19506802?dopt=abstract>  
CrossRef: <http://dx.doi.org/10.1007/s00018-009-0054-y>  
Google Scholar: [Author Only Title Only Author and Title](#)

**Couturier J, Koh CS, Zaffagnini M, Winger AM, Gualberto JM, Corbier C, Decottignies P, Jacquot JP, Lemaire SD, Didierjean C, Rouhier N (2009) Structure-function relationship of the chloroplastic glutaredoxin S12 with an atypical WCSYS active site. J Biol Chem 284: 9299-9310**

PubMed: <http://www.ncbi.nlm.nih.gov/pubmed/19158074?dopt=abstract>  
CrossRef: <http://dx.doi.org/10.1074/jbc.M807998200>  
Google Scholar: [Author Only Title Only Author and Title](#)

**Couturier J, Stroher E, Albetel AN, Roret T, Muthuramalingam M, Tarrago L, Seidel T, Tsan P, Jacquot JP, Johnson MK, Dietz KJ, Didierjean C, Rouhier N (2011) Arabidopsis chloroplastic glutaredoxin C5 as a model to explore molecular determinants for iron-sulfur cluster binding into glutaredoxins. J Biol Chem 286: 27515-27527**

PubMed: <http://www.ncbi.nlm.nih.gov/pubmed/21632542?dopt=abstract>  
CrossRef: <http://dx.doi.org/10.1074/jbc.M111.228726>  
Google Scholar: [Author Only Title Only Author and Title](#)

**Couturier J, Wu HC, Dhalleine T, Pégeot H, Sudre D, Gualberto JM, Jacquot JP, Gaynard F, Vignols F, Rouhier N (2014) Monothiol glutaredoxin-BolA interactions: redox control of Arabidopsis thaliana BolA2 and SufE1. Mol Plant 7: 187-205**

PubMed: <http://www.ncbi.nlm.nih.gov/pubmed/24203231?dopt=abstract>  
CrossRef: <http://dx.doi.org/10.1093/mp/sst156>  
Google Scholar: [Author Only Title Only Author and Title](#)

**Dolfini D, Gatta R, Mantovani R (2012) NF-Y and the transcriptional activation of CCAAT promoters. Critical Rev Biochem Mol Biol 47: 29-49**

PubMed: <http://www.ncbi.nlm.nih.gov/pubmed/22050321?dopt=abstract>  
CrossRef: <http://dx.doi.org/10.3109/10409238.2011.628970>  
Google Scholar: [Author Only Title Only Author and Title](#)

**Fish WW (1988) Rapid colorimetric micromethod for the quantitation of complexed iron in biological samples. Meth Enzymol 158: 357-364**

PubMed: <http://www.ncbi.nlm.nih.gov/pubmed/3374387?dopt=abstract>  
CrossRef: [http://dx.doi.org/10.1016/0076-6879\(88\)58067-9](http://dx.doi.org/10.1016/0076-6879(88)58067-9)  
Google Scholar: [Author Only Title Only Author and Title](#)

**Gama F, Keech O, Eymery F, Finkemeier I, Gelhaye E, Gardestrom P, Dietz KJ, Rey P, Jacquot JP, Rouhier N (2007) The mitochondrial type II peroxiredoxin from poplar. Physiol Plant 129: 196-206**

CrossRef: <http://dx.doi.org/10.1111/j.1399-3054.2006.00785.x>  
Google Scholar: [Author Only Title Only Author and Title](#)

**Guo Y, Huang C, Xie Y, Song F, Zhou X (2010) A tomato glutaredoxin gene SIGRX1 regulates plant responses to oxidative, drought and salt stresses. Planta 232: 1499-1509**

CrossRef: <http://dx.doi.org/10.1007/s00425-010-1271-1>  
Google Scholar: [Author Only Title Only Author and Title](#)

**Hunhorst P, Hanschmann EM, Bräutigam L, Stehling O, Hoffmann B, Mühlenhoff U, Lill R, Berndt C, Lillig CH (2013) Crucial function of vertebrate glutaredoxin 3 (PICOT) in iron homeostasis and hemoglobin maturation. Mol Biol Cell 24: 1895-1903**

PubMed: <http://www.ncbi.nlm.nih.gov/pubmed/23615448?dopt=abstract>  
CrossRef: <http://dx.doi.org/10.1091/mbc.E12-09-0648>  
Google Scholar: [Author Only Title Only Author and Title](#)

**Havaux M, Triantaphyllidès C, Genty B (2006) Autoluminescence imaging: a non-invasive tool for mapping oxidative stress. Trends Plant Sci 11: 480-484**

PubMed: <http://www.ncbi.nlm.nih.gov/pubmed/16956784?dopt=abstract>  
CrossRef: <http://dx.doi.org/10.1016/j.tplants.2006.08.001>  
Google Scholar: [Author Only Title Only Author and Title](#)

**Holtgreve S, Gohlke J, Starmann J, Druce S, Klocke S, Altmann B, Wojtera J, Lindermayr C, Scheibe R (2008) Regulation of plant cytosolic glyceraldehyde 3-phosphate dehydrogenase isoforms by thiol modifications. Physiol Plant 133: 211-228**

PubMed: <http://www.ncbi.nlm.nih.gov/pubmed/18298409?dopt=abstract>  
CrossRef: <http://dx.doi.org/10.1111/j.1399-3054.2008.01066.x>  
Google Scholar: [Author Only Title Only Author and Title](#)

**Hong L, Tang D, Zhu K, Wang K, Li M, Cheng Z (2012) Somatic and reproductive cell development in rice anther is regulated by a putative glutaredoxin. Plant Cell 24: 577-588**

CrossRef: <http://dx.doi.org/10.1105/tpc.111.093740>  
Google Scholar: [Author Only Title Only Author and Title](#)

**Hruz T, Laule O, Szabo G, Wessendorp F, Bleuler S, Oertle L, Widmayer P, Gruissem W, Zimmermann P (2008) Genevestigator v3: a reference expression database for the meta-analysis of transcriptomes. Ad Bioinformatics 2008: 420747**

PubMed: <http://www.ncbi.nlm.nih.gov/pubmed/19956698?dopt=abstract>  
Google Scholar: [Author Only Title Only Author and Title](#)

**Jbel M, Mercier A, Labbé S (2011) Grx4 monothiol glutaredoxin is required for iron limitation-dependent inhibition of Fep1. Eukaryotic Cell 10: 629-645**

CrossRef: <http://dx.doi.org/10.1128/EC.00015-11>  
Google Scholar: [Author Only](#) [Title Only](#) [Author and Title](#)

**Jiang K, Meng YL, Feldman LJ (2003) Quiescent center formation in maize roots is associated with an auxin-regulated oxidizing environment. Development 130: 1429-1438**

PubMed: <http://www.ncbi.nlm.nih.gov/pubmed/12588857?dopt=abstract>  
CrossRef: <http://dx.doi.org/10.1242/dev.00359>  
Google Scholar: [Author Only](#) [Title Only](#) [Author and Title](#)

**Kelliher T, Walbot V (2012) Hypoxia triggers meiotic fate acquisition in maize. Science 337: 345-348**

PubMed: <http://www.ncbi.nlm.nih.gov/pubmed/22822150?dopt=abstract>  
CrossRef: <http://dx.doi.org/10.1126/science.1220080>  
Google Scholar: [Author Only](#) [Title Only](#) [Author and Title](#)

**Kim S, Na JG, Hampsey M, Reinberg D (1997) The Dr1/DRAP1 heterodimer is a global repressor of transcription in vivo. Proc Natl Acad Sci USA 94: 820-825**

PubMed: <http://www.ncbi.nlm.nih.gov/pubmed/9023340?dopt=abstract>  
CrossRef: <http://dx.doi.org/10.1073/pnas.94.3.820>  
Google Scholar: [Author Only](#) [Title Only](#) [Author and Title](#)

**Kleinboelting N, Huet G, Kloetgen A, Viehoveer P, Weisshaar B (2012) GABI-Kat SimpleSearch: new features of the Arabidopsis thaliana T-DNA mutant database. Nucl Acids Res 40(D1): D1211-D1215**

PubMed: <http://www.ncbi.nlm.nih.gov/pubmed/22080561?dopt=abstract>  
Google Scholar: [Author Only](#) [Title Only](#) [Author and Title](#)

**Kumanovics A, Chen OS, Li L, Bagley D, Adkins EM, Lin H, Dingra NN, Outten CE, Keller G, Winge D, Ward DM, Kaplan J (2008) Identification of FRA1 and FRA2 as genes involved in regulating the yeast iron regulon in response to decreased mitochondrial iron-sulfur cluster synthesis. J Biol Chem 283: 10276-10286**

PubMed: <http://www.ncbi.nlm.nih.gov/pubmed/18281282?dopt=abstract>  
CrossRef: <http://dx.doi.org/10.1074/jbc.M801160200>  
Google Scholar: [Author Only](#) [Title Only](#) [Author and Title](#)

**Kumimoto RW, Adam L, Hymus GJ, Repetti PP, Reuber TL, Marion CM, Hempel FD, Ratcliffe OJ (2008) The nuclear factor Y subunits NF-YB2 and NF-YB3 play additive roles in the promotion of flowering by inductive long-day photoperiods in Arabidopsis. Planta 228: 709-723**

PubMed: <http://www.ncbi.nlm.nih.gov/pubmed/18600346?dopt=abstract>  
CrossRef: <http://dx.doi.org/10.1007/s00425-008-0773-6>  
Google Scholar: [Author Only](#) [Title Only](#) [Author and Title](#)

**Kumimoto RW, Zhang Y, Siefers N, Holt III BF (2010) NF-YC3, NF-YC4 and NF-YC9 are required for CONSTANS-mediated, photoperiod-dependent flowering in Arabidopsis thaliana. Plant J 63: 379-391**

Google Scholar: [Author Only](#) [Title Only](#) [Author and Title](#)

**La Camera S, L'Haridon F, Astier J, Zander M, Abou-Mansour E, Page G, Thurow C, Wendehenne D, Gatz C, Metraux JP, Lamotte O (2011) The glutaredoxin ATGRXS13 is required to facilitate Botrytis cinerea infection of Arabidopsis thaliana plants. Plant J 68: 507-519**

PubMed: <http://www.ncbi.nlm.nih.gov/pubmed/21756272?dopt=abstract>  
CrossRef: <http://dx.doi.org/10.1111/j.1365-3113X.2011.04706.x>  
Google Scholar: [Author Only](#) [Title Only](#) [Author and Title](#)

**Laloum T, De Mita S, Gamas P, Baudin M, Niebel A (2013) CCAAT-box binding transcription factors in plants: Y so many? Trends Plant Sci 18: 157-166**

PubMed: <http://www.ncbi.nlm.nih.gov/pubmed/22939172?dopt=abstract>  
CrossRef: <http://dx.doi.org/10.1016/j.tplants.2012.07.004>  
Google Scholar: [Author Only](#) [Title Only](#) [Author and Title](#)

**Laporte D, Olate E, Salinas P, Salazar M, Jordana X, Holuigue L (2012) Glutaredoxin GRXS13 plays a key role in protection against photooxidative stress in Arabidopsis. J Exp Bot 63: 503-515**

PubMed: <http://www.ncbi.nlm.nih.gov/pubmed/21963612?dopt=abstract>  
CrossRef: <http://dx.doi.org/10.1093/jxb/err301>  
Google Scholar: [Author Only](#) [Title Only](#) [Author and Title](#)

**Levy YY, Dean C (1998) The transition to flowering. Plant Cell 10:1973-1989**

PubMed: <http://www.ncbi.nlm.nih.gov/pubmed/9836739?dopt=abstract>  
CrossRef: <http://dx.doi.org/10.1105/tpc.10.12.1973>  
Google Scholar: [Author Only](#) [Title Only](#) [Author and Title](#)

**Lillig CH, Berndt C, Vergnolle O, Lonn ME, Hudemann C, Bill E, Holmgren A (2005) Characterization of human glutaredoxin 2 as iron-sulfur protein: a possible role as redox sensor. Proc Natl Acad Sci USA 102: 8168-8173**

PubMed: <http://www.ncbi.nlm.nih.gov/pubmed/15917333?dopt=abstract>  
CrossRef: <http://dx.doi.org/10.1073/pnas.0500735102>  
Google Scholar: [Author Only](#) [Title Only](#) [Author and Title](#)

**Marchal C, Delorme-Hinoux V, Bariat L, Siala W, Belin C, Saez-Vasquez J, Riondet C, Reichheld JP (2014) NTR/NRX define a new thioredoxin system in the nucleus of Arabidopsis thaliana cells. Mol Plant 7: 30-44**

PubMed: <http://www.ncbi.nlm.nih.gov/pubmed/24253198?dopt=abstract>  
CrossRef: <http://dx.doi.org/10.1093/mp/sst162>  
Google Scholar: [Author Only](#) [Title Only](#) [Author and Title](#)

**Mercier A, Labbé S (2009) Both Php4 function and subcellular localization are regulated by iron via a multistep mechanism involving the glutaredoxin Grx4 and the exportin Crm1. J Biol Chem 284: 20249-20262**

PubMed: <http://www.ncbi.nlm.nih.gov/pubmed/19502236?dopt=abstract>

CrossRef: <http://dx.doi.org/10.1074/jbc.M109.009563>

Google Scholar: [Author Only](#) [Title Only](#) [Author and Title](#)

**Meyer Y, Buchanan BB, Vignols F, Reichheld JP (2009) Thioredoxins and glutaredoxins: unifying elements in redox biology. Ann Rev Genet 43: 335-367**

PubMed: <http://www.ncbi.nlm.nih.gov/pubmed/19691428?dopt=abstract>

CrossRef: <http://dx.doi.org/10.1146/annurev-genet-102108-134201>

Google Scholar: [Author Only](#) [Title Only](#) [Author and Title](#)

**Michelet L, Zaffagnini M, Marchand C, Collin V, Decottignies P, Tsan P, Lancelin JM, Trost P, Miginiac-Maslow M, Noctor G, Lemaire SD (2005) Glutathionylation of chloroplast thioredoxin f is a redox signaling mechanism in plants. Proc Natl Acad Sci USA 102: 16478-16483**

PubMed: <http://www.ncbi.nlm.nih.gov/pubmed/16263928?dopt=abstract>

CrossRef: <http://dx.doi.org/10.1073/pnas.0507498102>

Google Scholar: [Author Only](#) [Title Only](#) [Author and Title](#)

**Molina MM, Belli G, de la Torre MA, Rodriguez-Manzanique MT, Herrero E (2004) Nuclear monothiol glutaredoxins of *Saccharomyces cerevisiae* can function as mitochondrial glutaredoxins. J Biol Chem 279: 51923-51930**

PubMed: <http://www.ncbi.nlm.nih.gov/pubmed/15456753?dopt=abstract>

CrossRef: <http://dx.doi.org/10.1074/jbc.M410219200>

Google Scholar: [Author Only](#) [Title Only](#) [Author and Title](#)

**Mühlenhoff U, Gerber J, Richhardt N, Lill R (2003) Components involved in assembly and dislocation of iron-sulfur clusters on the scaffold protein Isu1p. EMBO J 22: 4815-4825**

PubMed: <http://www.ncbi.nlm.nih.gov/pubmed/12970193?dopt=abstract>

CrossRef: <http://dx.doi.org/10.1093/emboj/cdg446>

Google Scholar: [Author Only](#) [Title Only](#) [Author and Title](#)

**Mühlenhoff U, Molik S, Godoy JR, Uzarska MA, Richter N, Seubert A, Zhang Y, Stubbe J, Pierrel F, Herrero E, Lillig CH, Lill R (2010) Cytosolic monothiol glutaredoxins function in intracellular iron sensing and trafficking via their bound iron-sulfur cluster. Cell Metab 12: 373-385**

PubMed: <http://www.ncbi.nlm.nih.gov/pubmed/20889129?dopt=abstract>

CrossRef: <http://dx.doi.org/10.1016/j.cmet.2010.08.001>

Google Scholar: [Author Only](#) [Title Only](#) [Author and Title](#)

**Murmu J, Bush MJ, DeLong C, Li S, Xu M, Khan M, Malcolmson C, Fobert PR, Zachgo S, Hepworth SR (2010) Arabidopsis basic leucine-zipper transcription factors TGA9 and TGA10 interact with floral glutaredoxins ROXY1 and ROXY2 and are redundantly required for anther development. Plant Physiol 154: 1492-1504**

PubMed: <http://www.ncbi.nlm.nih.gov/pubmed/20805327?dopt=abstract>

CrossRef: <http://dx.doi.org/10.1104/pp.110.159111>

Google Scholar: [Author Only](#) [Title Only](#) [Author and Title](#)

**Nakshatri H, Bhat-Nakshatri P, Currie RA (1996) Subunit association and DNA binding activity of the heterotrimeric transcription factor NF-Y is regulated by cellular redox. J Biol Chem 271: 28784-28791**

PubMed: <http://www.ncbi.nlm.nih.gov/pubmed/8910521?dopt=abstract>

CrossRef: <http://dx.doi.org/10.1074/jbc.271.46.28784>

Google Scholar: [Author Only](#) [Title Only](#) [Author and Title](#)

**Ndamukong I, Abdallat AA, Thurow C, Fode B, Zander M, Weigel R, Gatz C (2007) SA-inducible Arabidopsis glutaredoxin interacts with TGA factors and suppresses JA-responsive PDF1.2 transcription. Plant J 50: 128-139**

PubMed: <http://www.ncbi.nlm.nih.gov/pubmed/17397508?dopt=abstract>

Google Scholar: [Author Only](#) [Title Only](#) [Author and Title](#)

**Nelissen H, Clarke JH, De Block M, De Block S, Vanderhaeghen R, Zielinski RE, Dyer T, Lust S, Inzé D, Van Lijsebettens M (2003) DRL1, a homolog of the yeast TOT4/KT12 protein, has a function in meristem activity and organ growth in plants. Plant Cell 15: 639-654**

PubMed: <http://www.ncbi.nlm.nih.gov/pubmed/12615938?dopt=abstract>

Google Scholar: [Author Only](#) [Title Only](#) [Author and Title](#)

**Nelissen H, De Groeve S, Fleury D, Neyt P, Bruno L, Bitonti MB, Vandenbussche F, Van der Straeten D, Yamaguchi T, Tsukaya H, Witters E, De Jaeger G, Houben A, Van Lijsebettens M (2010) Plant Elongator regulates auxin-related genes during RNA polymerase II transcription elongation. Proc Natl Acad Sci USA 107: 1678-1683**

PubMed: <http://www.ncbi.nlm.nih.gov/pubmed/20080602?dopt=abstract>

CrossRef: <http://dx.doi.org/10.1073/pnas.0913559107>

Google Scholar: [Author Only](#) [Title Only](#) [Author and Title](#)

**Nelissen H, Fleury D, Bruno L, Robles P, De Veylder L, Traas J, Micol JL, Van Montagu M, Inzé D, Van Lijsebettens M (2005) The elongata mutants identify a functional Elongator complex in plants with a role in cell proliferation during organ growth. Proc Natl Acad Sci USA 102: 7754-7759**

CrossRef: <http://dx.doi.org/10.1073/pnas.0502600102>

Google Scholar: [Author Only](#) [Title Only](#) [Author and Title](#)

**Ojeda L, Keller G, Mühlenhoff U, Rutherford JC, Lill R, Winge DR (2006) Role of glutaredoxin-3 and glutaredoxin-4 in the iron regulation of the Aft1 transcriptional activator in *Saccharomyces cerevisiae*. J Biol Chem 281: 17661-17669**

CrossRef: <http://dx.doi.org/10.1074/jbc.M602165200>

Google Scholar: [Author Only](#) [Title Only](#) [Author and Title](#)

**Petroni K, Kumimoto RW, Gnesutta N, Calvenzani V, Fornari M, Tonelli C, Holt III BF, Mantovani R (2012) The promiscuous life of plant NUCLEAR FACTOR Y transcription factors. *Plant Cell* 24: 4777-4792**

PubMed: <http://www.ncbi.nlm.nih.gov/pubmed/23275578?dopt=abstract>

CrossRef: <http://dx.doi.org/10.1105/tpc.112.105734>

Google Scholar: [Author Only Title Only Author and Title](#)

**Pierik AJ, Netz DJ, Lill R (2009) Analysis of iron-sulfur protein maturation in eukaryotes. *Nature Protocols* 4: 753-766**

PubMed: <http://www.ncbi.nlm.nih.gov/pubmed/19528951?dopt=abstract>

CrossRef: <http://dx.doi.org/10.1038/nprot.2009.39>

Google Scholar: [Author Only Title Only Author and Title](#)

**Pontvianne F, Abou-Ellail M, Douet J, Comella P, Matia I, Chandrasekhara C, Debures A, Blevins T, Cooke R, Medina FJ, Tourmente S, Pikaard CS, Sáez-Vásquez J (2010) Nucleolin is required for DNA methylation state and the expression of rRNA gene variants in *Arabidopsis thaliana*. *PLoS Genet* 6: e1001225**

PubMed: <http://www.ncbi.nlm.nih.gov/pubmed/21124873?dopt=abstract>

Google Scholar: [Author Only Title Only Author and Title](#)

**Pujol-Carrion N, Belli G, Herrero E, Nogues A, de la Torre-Ruiz MA (2006) Glutaredoxins Grx3 and Grx4 regulate nuclear localisation of Aft1 and the oxidative stress response in *Saccharomyces cerevisiae*. *J Cell Sci* 119: 4554-4564**

PubMed: <http://www.ncbi.nlm.nih.gov/pubmed/17074835?dopt=abstract>

CrossRef: <http://dx.doi.org/10.1242/jcs.03229>

Google Scholar: [Author Only Title Only Author and Title](#)

**Qin Y, Leydon AR, Manziello A, Pandey R, Mount D, Denic S, Vasic B, Johnson MA, Palanivelu R (2009) Penetration of the stigma, style elicits a novel transcriptome in pollen tubes, pointing to genes critical for growth in a pistil. *PLoS Genet* 8: e1000621**

PubMed: <http://www.ncbi.nlm.nih.gov/pubmed/19714218?dopt=abstract>

Google Scholar: [Author Only Title Only Author and Title](#)

**Rey P, Cuine S, Eymery F, Garin J, Court M, Jacquot JP, Rouhier N, Broin M (2005) Analysis of the proteins targeted by CDSP32, a plastidic thioredoxin participating in oxidative stress responses. *Plant J* 41: 31-42**

PubMed: <http://www.ncbi.nlm.nih.gov/pubmed/15610347?dopt=abstract>

Google Scholar: [Author Only Title Only Author and Title](#)

**Riondet C, Desourisn JP, Montoyan JG, Chartier Y, Meyer Y, Reichheld JP (2012) A dicotyledon-specific glutaredoxin GRXC1 family with dimer-dependent redox regulation is functionally redundant with GRXC2. *Plant Cell Environ* 35: 360-373**

PubMed: <http://www.ncbi.nlm.nih.gov/pubmed/21767278?dopt=abstract>

CrossRef: <http://dx.doi.org/10.1111/j.1365-3040.2011.02355.x>

Google Scholar: [Author Only Title Only Author and Title](#)

**Robinson JB Jr, Inman L, Sumegi B, Sreere PA (1987) Further characterization of the Krebs tricarboxylic acid cycle metabolon. *J Biol Chem* 262: 1786-1790**

PubMed: <http://www.ncbi.nlm.nih.gov/pubmed/2433288?dopt=abstract>

Google Scholar: [Author Only Title Only Author and Title](#)

**Rodriguez-Manzanares MT, Tamarit J, Belli G, Ros J, Herrero E (2002) Grx5 is a mitochondrial glutaredoxin required for the activity of iron/sulfur enzymes. *Mol Biol Cell* 13: 1109-1121**

PubMed: <http://www.ncbi.nlm.nih.gov/pubmed/11950925?dopt=abstract>

CrossRef: <http://dx.doi.org/10.1091/mbc.01-10-0517>

Google Scholar: [Author Only Title Only Author and Title](#)

**Rouhier N, Couturier J, Jacquot JP (2006) Genome-wide analysis of plant glutaredoxin systems. *J Exp Bot* 57: 1685-1696**

PubMed: <http://www.ncbi.nlm.nih.gov/pubmed/16720602?dopt=abstract>

CrossRef: <http://dx.doi.org/10.1093/jxb/erl001>

Google Scholar: [Author Only Title Only Author and Title](#)

**Rouhier N, Couturier J, Johnson MK, Jacquot JP (2010) Glutaredoxins: roles in iron homeostasis. *Trends Biochem Sci* 35: 43-52**

PubMed: <http://www.ncbi.nlm.nih.gov/pubmed/19811920?dopt=abstract>

CrossRef: <http://dx.doi.org/10.1016/j.tibs.2009.08.005>

Google Scholar: [Author Only Title Only Author and Title](#)

**Rouhier N, Gelhaye E, Sautiere PE, Brun A, Laurent P, Tagu D, Gerard J, de Fay E, Meyer Y, Jacquot JP (2001) Isolation and characterization of a new peroxiredoxin from poplar sieve tubes that uses either glutaredoxin or thioredoxin as a proton donor. *Plant Physiol* 127: 1299-1309**

PubMed: <http://www.ncbi.nlm.nih.gov/pubmed/11706208?dopt=abstract>

CrossRef: <http://dx.doi.org/10.1104/pp.010586>

Google Scholar: [Author Only Title Only Author and Title](#)

**Rouhier N, Lemaire SD, Jacquot JP (2008) The role of glutathione in photosynthetic organisms: emerging functions for glutaredoxins and glutathionylation. *Annual Rev Plant Biol* 59: 143-166**

PubMed: <http://www.ncbi.nlm.nih.gov/pubmed/18444899?dopt=abstract>

CrossRef: <http://dx.doi.org/10.1146/annurev.arplant.59.032607.092811>

Google Scholar: [Author Only Title Only Author and Title](#)

**Rouhier N, Unno H, Bandyopadhyay S, Masip L, Kim SK, Hirasawa M, Gualberto JM, Lattard V, Kusunoki M, Knaff DB, Georgiou G, Hase T, Johnson MK, Jacquot JP (2007) Functional, structural, and spectroscopic characterization of a glutathione-ligated [2Fe-2S] cluster in poplar glutaredoxin C1. *Proc Natl Acad Sci USA* 104: 7379-7384**

PubMed: <http://www.ncbi.nlm.nih.gov/pubmed/17460036?dopt=abstract>

CrossRef: <http://dx.doi.org/10.1073/pnas.0702268104>

Google Scholar: [Author Only Title Only Author and Title](#)

**Schaedler TA, Thornton JD, Kruse I, Schwarzländer M, Meyer AJ, van Veen HW, Balk J (2014) A conserved mitochondrial ATP-binding cassette transporter exports glutathione polysulfide for cytosolic metal cofactor assembly. J Biol Chem 289: 23264-23274**

PubMed: <http://www.ncbi.nlm.nih.gov/pubmed/25006243?dopt=abstract>

CrossRef: <http://dx.doi.org/10.1074/jbc.M114.553438>

Google Scholar: [Author Only Title Only Author and Title](#)

**Song W, Solimeo H, Rupert RA, Yadav NS, Zhu Q (2002) Functional dissection of a rice Dr1/DrAp1 transcriptional repression complex. Plant Cell 14: 181-195**

PubMed: <http://www.ncbi.nlm.nih.gov/pubmed/11826307?dopt=abstract>

CrossRef: <http://dx.doi.org/10.1105/tpc.010320>

Google Scholar: [Author Only Title Only Author and Title](#)

**Sundaram S, Rathinasabapathi B (2010) Transgenic expression of fern *Pteris vittata* glutaredoxin PvGrx5 in *Arabidopsis thaliana* increases plant tolerance to high temperature stress and reduces oxidative damage to proteins. Planta 231: 361-369**

PubMed: <http://www.ncbi.nlm.nih.gov/pubmed/19936779?dopt=abstract>

CrossRef: <http://dx.doi.org/10.1007/s00425-009-1055-7>

Google Scholar: [Author Only Title Only Author and Title](#)

**Sundaram S, Rathinasabapathi B, Ma LQ, Rosen BP (2008) An arsenate-activated glutaredoxin from the arsenic hyperaccumulator fern *Pteris vittata* L. regulates intracellular arsenite J Biol Chem 283: 6095-6101**

PubMed: <http://www.ncbi.nlm.nih.gov/pubmed/18156657?dopt=abstract>

Google Scholar: [Author Only Title Only Author and Title](#)

**Tarrago L, Laugier E, Zaffagnini M, Marchand C, Le Marechal P, Rouhier N, Lemaire SD, Rey P (2009) Regeneration mechanisms of *Arabidopsis thaliana* methionine sulfoxide reductases B by glutaredoxins and thioredoxins. J Biol Chem 284: 18963-18971**

PubMed: <http://www.ncbi.nlm.nih.gov/pubmed/19457862?dopt=abstract>

CrossRef: <http://dx.doi.org/10.1074/jbc.M109.015487>

Google Scholar: [Author Only Title Only Author and Title](#)

**Vernoux T, Wilson RC, Seeley KA, Reichheld JP, Muroy S, Brown S, Maughan SC, Cobbett CS, Van Montagu M, Inzé D, May MJ, Sung ZR (2000) The ROOT MERISTEMLESS1/CADMIUM SENSITIVE2 gene defines a glutathione-dependent pathway involved in initiation and maintenance of cell division during postembryonic root development. Plant Cell 12: 97-110**

PubMed: <http://www.ncbi.nlm.nih.gov/pubmed/10634910?dopt=abstract>

CrossRef: <http://dx.doi.org/10.1105/tpc.12.1.97>

Google Scholar: [Author Only Title Only Author and Title](#)

**Waszczak C, Akter S, Eeckhout D, Persiau G, Wahni K, Bodra N, Van Molle I, De Smet B, Vertommen D, Gevaert K, De Jaeger G, Van Montagu M, Messens J, Van Breusegem F (2014) Sulfenome mining in *Arabidopsis thaliana*. Proc Natl Acad Sci USA 11: 11545-11550**

PubMed: <http://www.ncbi.nlm.nih.gov/pubmed/25049418?dopt=abstract>

CrossRef: <http://dx.doi.org/10.1073/pnas.1411607111>

Google Scholar: [Author Only Title Only Author and Title](#)

**Wojtera-Kwiczor J, Groß F, Leffers HM, Kang M, Schneider M, Scheibe R (2013) Transfer of a redox-signal through the cytosol by redox-dependent microcompartmentation of glycolytic enzymes at mitochondria and actin cytoskeleton. Front Plant Sci 3: 284**

PubMed: <http://www.ncbi.nlm.nih.gov/pubmed/23316205?dopt=abstract>

Google Scholar: [Author Only Title Only Author and Title](#)

**Wu Q, Lin J, Liu JZ, Wang X, Lim W, Oh M, Park J, Rajashekar CB, Whitham SA, Cheng NH, Hirschi KD, Park S (2012) Ectopic expression of *Arabidopsis* glutaredoxin AtGRXS17 enhances thermotolerance in tomato. Plant Biotechnol J 10: 945-955**

PubMed: <http://www.ncbi.nlm.nih.gov/pubmed/22762155?dopt=abstract>

CrossRef: <http://dx.doi.org/10.1111/j.1467-7652.2012.00723.x>

Google Scholar: [Author Only Title Only Author and Title](#)

**Xing S, Zachgo S (2008) ROXY1 and ROXY2, two *Arabidopsis* glutaredoxin genes, are required for anther development. Plant J 53: 790-801**

PubMed: <http://www.ncbi.nlm.nih.gov/pubmed/18036205?dopt=abstract>

Google Scholar: [Author Only Title Only Author and Title](#)

**Yu X, Pasternak T, Eiblmeier M, Ditengou F, Kochersperger P, Sun J, Wang H, Rennenberg H, Teale W, Paponov I, Zhou W, Li C, Li X, Palme K (2013) Plastid-localized glutathione reductase2-regulated glutathione redox status is essential for *Arabidopsis* root apical meristem maintenance. Plant Cell 25: 4451-4468**

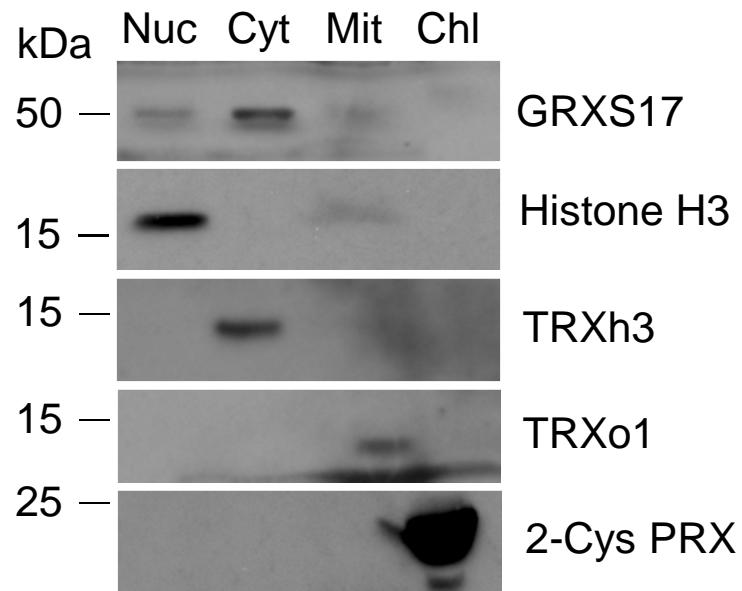
PubMed: <http://www.ncbi.nlm.nih.gov/pubmed/24249834?dopt=abstract>

CrossRef: <http://dx.doi.org/10.1105/tpc.113.117028>

Google Scholar: [Author Only Title Only Author and Title](#)



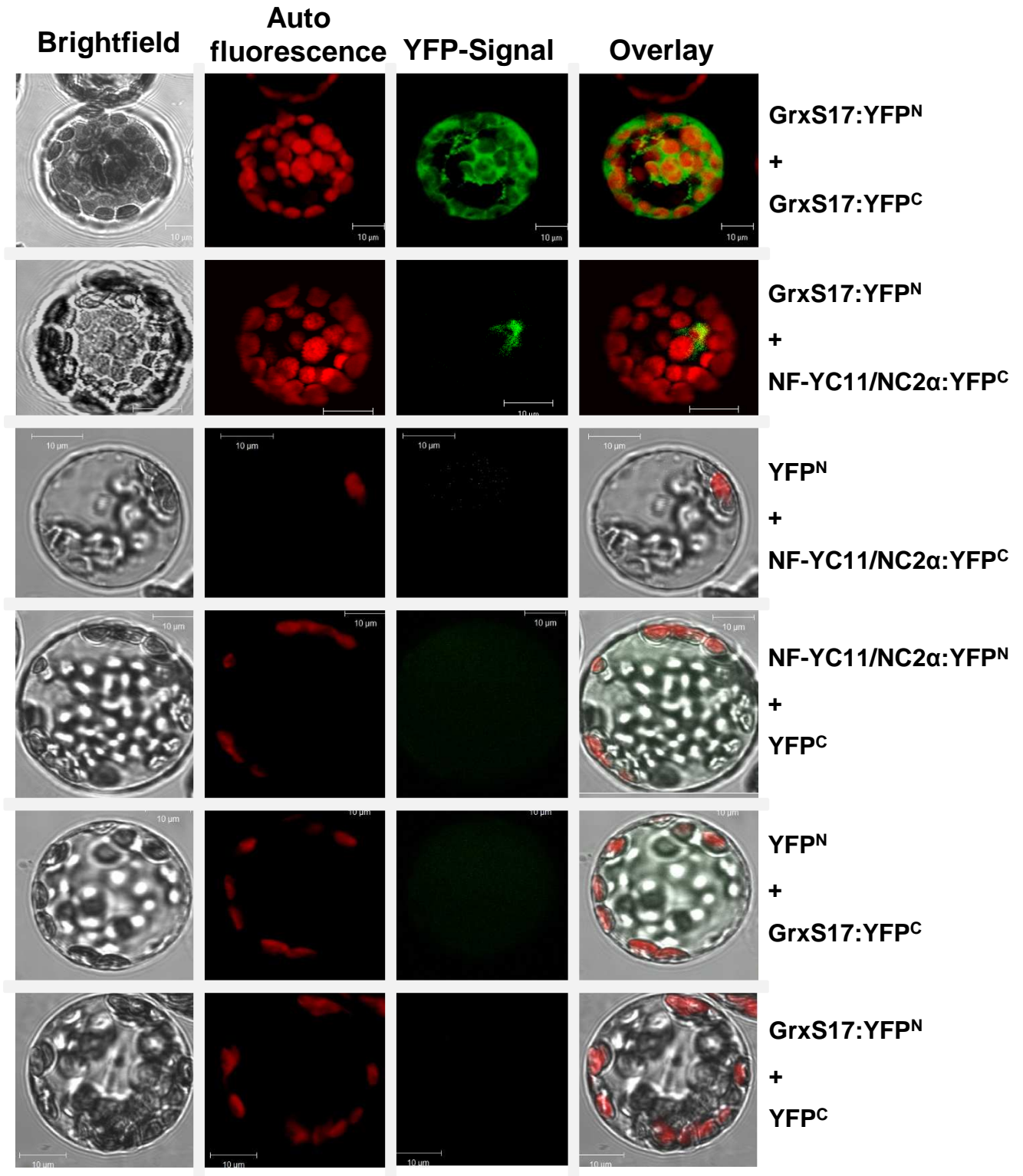
Figure S2



**Figure S2. Subcellular localization of GRXS17.**

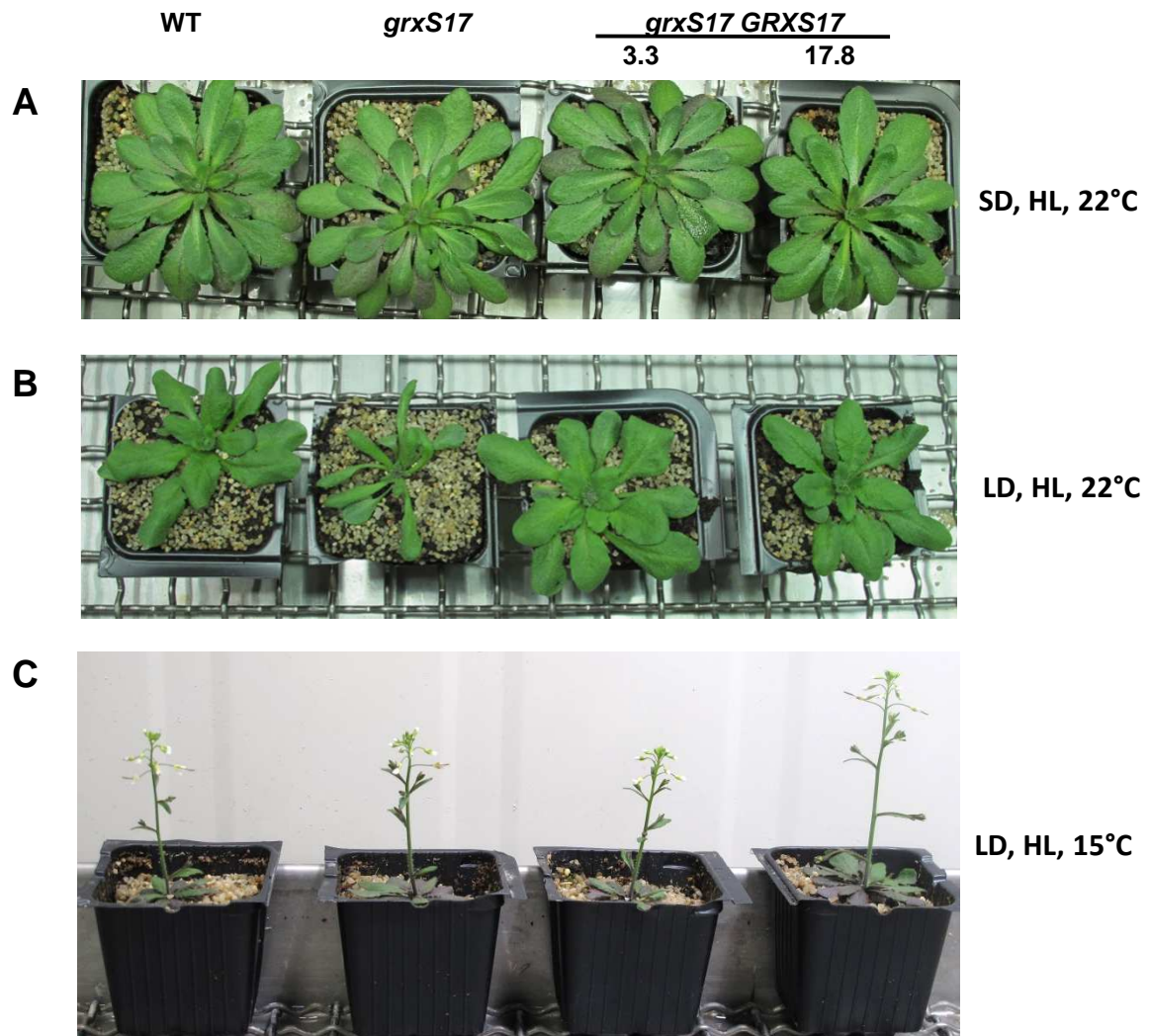
Immunodetection of GRXS17, nuclear histone H3, cytosolic thioredoxin h3 (TRXh3), mitochondrial thioredoxin o1 (TRXo1) and plastidial 2-Cys peroxiredoxin (2-Cys PRX) in nuclear (Nuc), cytosolic (Cyt), mitochondrial (Mit) and chloroplastic (Chl) fractions prepared from Arabidopsis plants. The faint histone H3 band detected in mitochondrial fraction probably indicates a slight contamination from nuclei.

Figure S3



**Figure S3. Controls of the bimolecular fluorescence complementation assay of GRXS17 and NF-YC11/NC2α.** Vectors encoding C- and N-terminal split-YFP fusions with GRXS17 or NF-YC11/NC2α and empty vectors were co-transformed into *A. thaliana* mesophyll protoplasts. Pictures were taken 14 h after transformation.

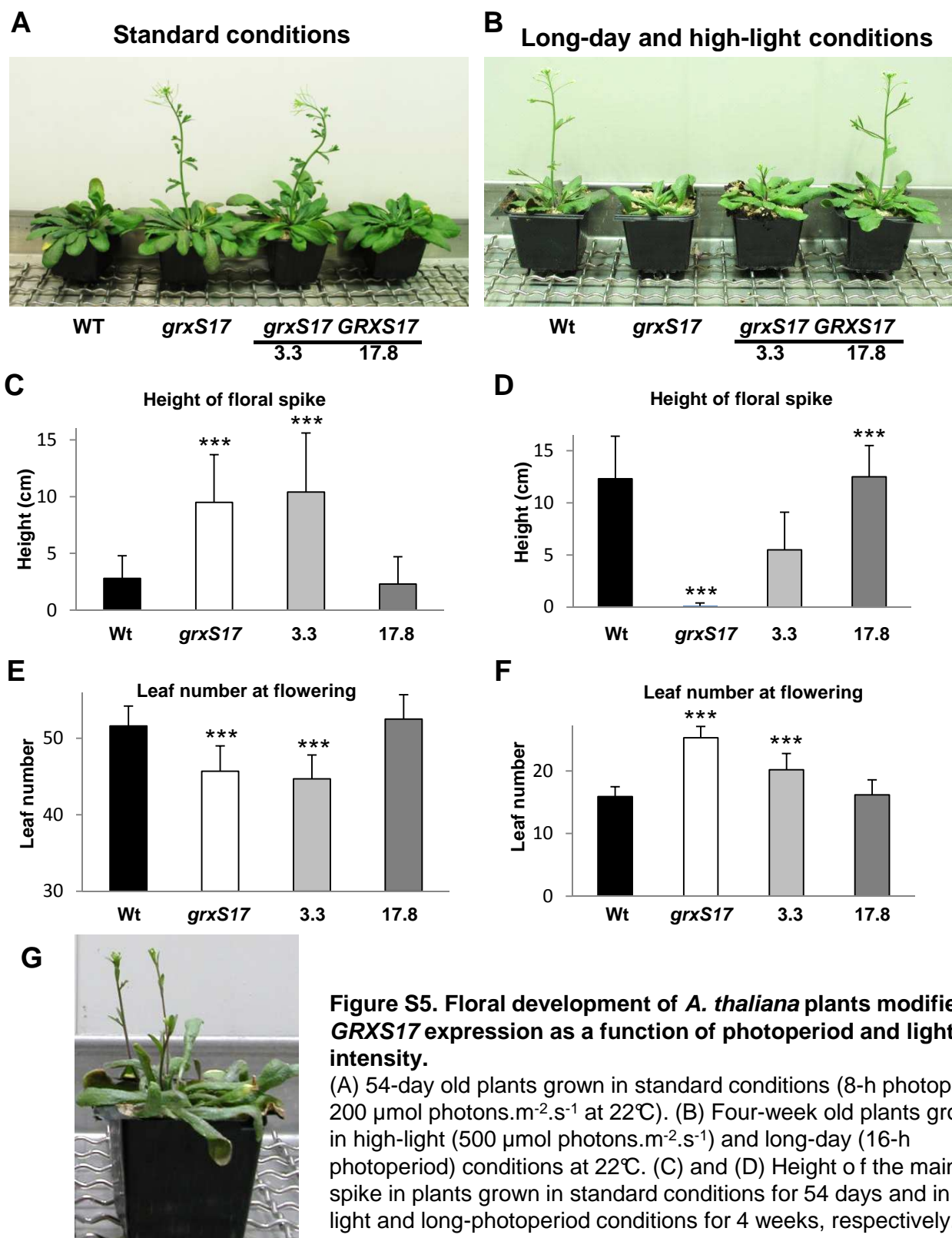
Figure S4



**Figure S4. Growth and development of *A. thaliana* plants modified in *GRXS17* expression as a function of light and temperature regimes.**

(A) Five-week old plants grown for 2 weeks in standard conditions and then transferred for 3 weeks to high-light (500  $\mu\text{mol photons.m}^{-2}.\text{s}^{-1}$ ) and short-day (8-h photoperiod) conditions at 22°C. (B) Three-week old plants grown in high-light (500  $\mu\text{mol photons.m}^{-2}.\text{s}^{-1}$ ) and long-day (16-h photoperiod) conditions at 22°C. (C) Seven-week old plants grown for 3 weeks in standard conditions and then transferred to 15°C, long-day photoperiod (16 h) and high-light conditions (500  $\mu\text{mol photons.m}^{-2}.\text{s}^{-1}$ ) for 4 weeks. WT, wild-type plants; *grxS17*, homozygous SALK\_021301 plants; *grxS17 GRXS17* 3.3 and 17.8, two independent KO lines expressing *GRXS17*.

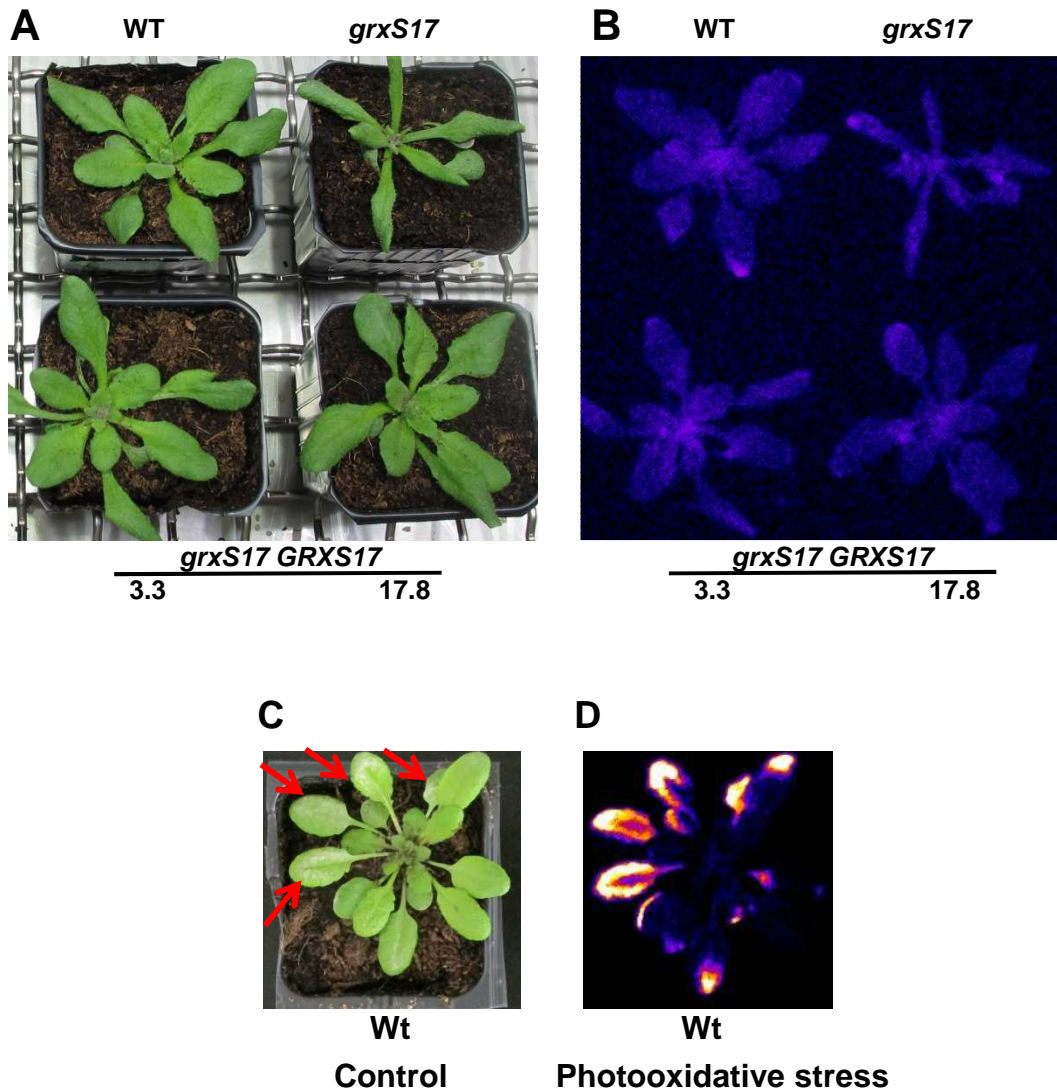
Figure S5



**Figure S5. Floral development of *A. thaliana* plants modified in *GRXS17* expression as a function of photoperiod and light intensity.**

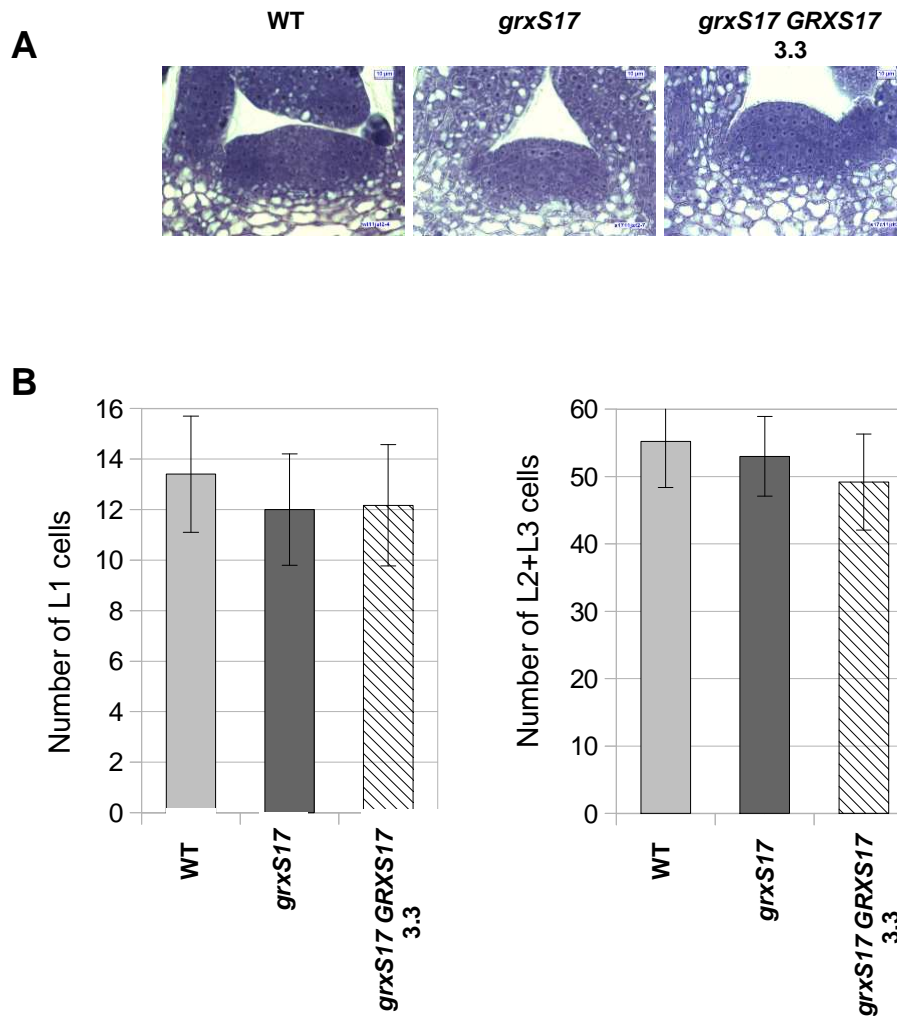
(A) 54-day old plants grown in standard conditions (8-h photoperiod, 200  $\mu\text{mol photons}\cdot\text{m}^{-2}\cdot\text{s}^{-1}$  at 22°C). (B) Four-week old plants grown in high-light (500  $\mu\text{mol photons}\cdot\text{m}^{-2}\cdot\text{s}^{-1}$ ) and long-day (16-h photoperiod) conditions at 22°C. (C) and (D) Height of the main floral spike in plants grown in standard conditions for 54 days and in high-light and long-photoperiod conditions for 4 weeks, respectively. (E) and (F) Number of leaves at flowering in plants grown in standard conditions and in high-light and long-day conditions, respectively. (G) Five-week old *grxS17* plant grown in high-light (500  $\mu\text{mol photons}\cdot\text{m}^{-2}\cdot\text{s}^{-1}$ ) and long-day (16-h photoperiod) conditions at 22°C. WT, Wild-type plants; *grxS17*, homozygous SALK\_021301 plants; *grxS17 GRXS17* 3.3 and 17.8, two independent KO lines expressing *GRXS17*. \*\*\*, significantly different from the WT value with  $p < 0.01$  (t test).

Figure S6



**Figure S6. Autoluminescence in *A. thaliana* plants modified in *GRXS17* expression.** (A) Three-week old plants grown in high-light ( $500 \mu\text{mol photons.m}^{-2}.\text{s}^{-1}$ ) and long-day (16-h photoperiod) conditions at  $22^\circ\text{C}$ . (B) Autoluminescence imaging of lipid peroxidation in these plants. The homogeneous blue/purple color of plants indicates the absence of photodamage (compare panel D for positive control). WT, wild-type plants; *grxS17*, homozygous SALK\_021301 plants; *grxS17 GRXS17* 3.3 and 17.8, two independent KO lines expressing *GRXS17*. (C) Five-week old WT plant grown in standard conditions (8-h photoperiod,  $200 \mu\text{mol photons.m}^{-2}.\text{s}^{-1}$  at  $22^\circ\text{C}$ ) and then exposed to a photooxidative treatment for 1 day (8-h photoperiod,  $1250 \mu\text{mol photons.m}^{-2}.\text{s}^{-1}$  at  $6^\circ\text{C}$ ). The red arrows indicate leaves displaying bleaching resulting from photodamage. (D) Autoluminescence imaging of lipid peroxidation in the plant shown in panel C. The damaged leaves appear in white/yellow color due to the photon emission associated with lipid peroxidation.

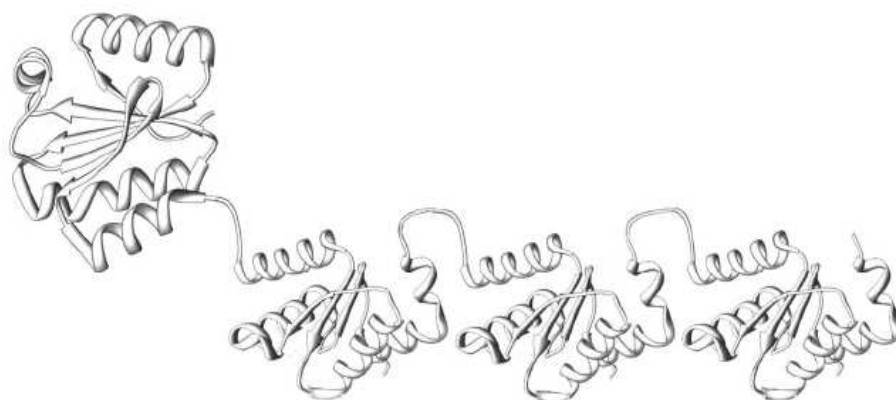
# Figure S7



**Figure S7. Structure of the shoot apical meristem (SAM) in the *grxS17* mutant.**

(A) Histological structure of the SAM stained by toluidine blue in WT, *grxS17* and *grxS17 GRXS17* (line 3.3) seedlings grown for 11 days in short-day (8 h) conditions and standard light ( $200 \mu\text{mol photons}\cdot\text{m}^{-2}\cdot\text{s}^{-1}$ ). (B) Number of L1, L2 and L3 layer stem cells in cross-sections of SAM shown in (A). Ten sections per genotype were analyzed.

Figure S8



```

M2 MLFMKGIPEEPCRGFSRKVVDILKEVNVDFGSFDILSDNEVREGLKKFSNWPTFPQLYCN 226
M3 MLFMKGRPEEPKCGFSGKVVEILNQEKIEFGSFDILLDDEVQRGLKVYSNWSSYPQLYVK 356
M4 MLFMKGPDEPKCGFSSKVVKALRGENVSFGSFDILTDEEVRQGIKNFSNWPTFPQLYYK 463
***** *:***:***** ***. * . :.:***** *:***:*** :***. :.:***** :
M2 GELGGADIAIAMHESGELKDAFKD 251
M3 GELMGGSDIVLEMQKSGELKKVLTE 381
M4 GELIGGCDIIMELSESGDLKATLSE 488
***:***.*** : : :***:*** .:.:

```

**Figure S8. Hypothetical structure of GRXS17 and amino acid alignment of the three GRX domains M2, M3 and M4 from *A. thaliana*.** The structures of the single domains were generated from 1XFL and 3L4N pdb entries for TRX and GRX proteins, respectively, and are not experimentally confirmed. The linker regions and the relative positions of the TRX domain are speculative.

## Figure S9

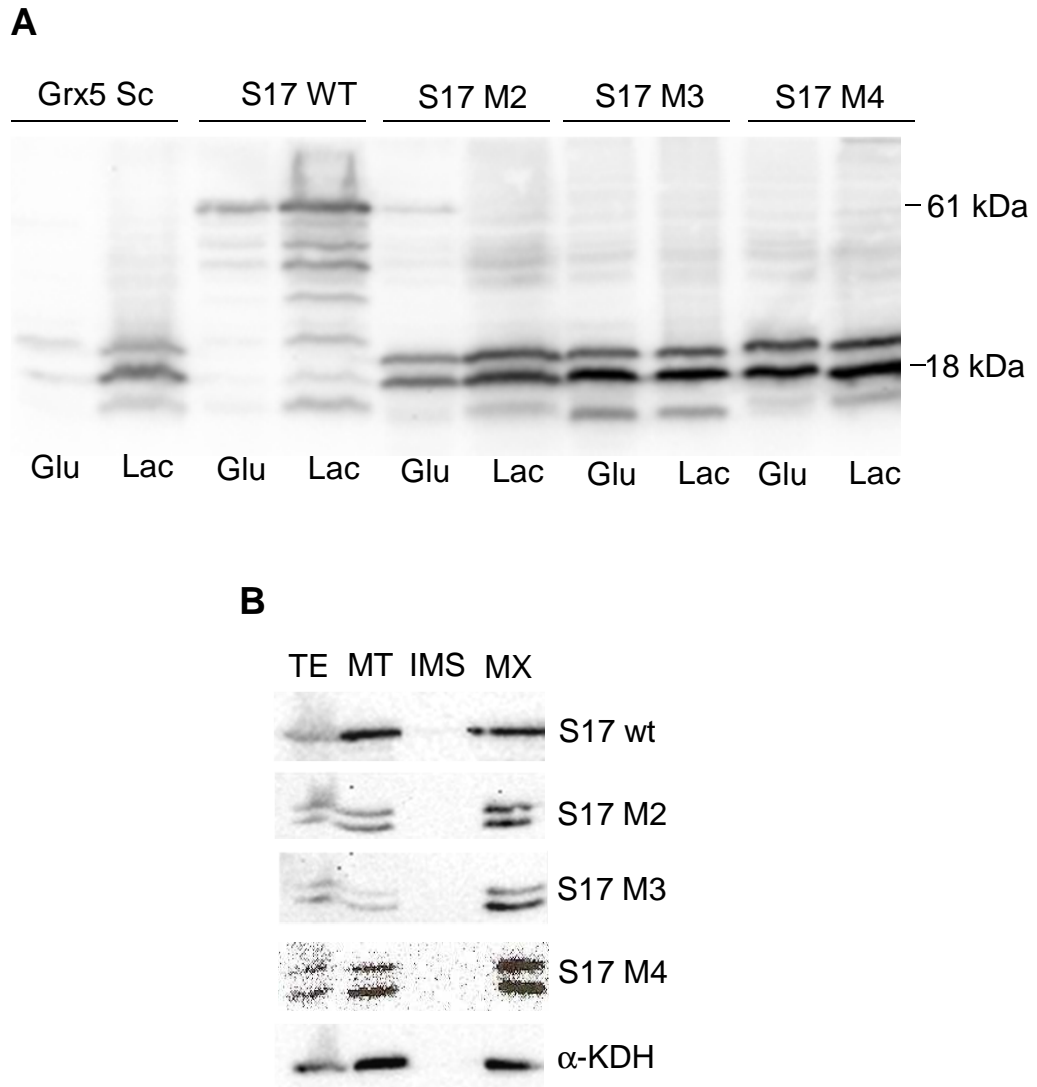


### Figure S9. Analysis of the GRXS17 forms expressed in *S. cerevisiae*.

(A) Western blot analysis with anti-HA antibodies (10  $\mu$ g total proteins from cell extracts per lane). Extracts from yeast cells expressing the homologous GRX5 protein under the native promoter (Grx5 Sc) are included as control. Samples from cells grown in fermentative conditions (Glu) and in respiratory conditions (Lac) were run in parallel. Molecular size of the expressed S17 forms is indicated. (B) Subfractionation of extracts from *S. cerevisiae* cells expressing the respective S17 forms and grown in respiratory conditions (lactose medium). TE (total extracts, 25  $\mu$ g), MT (total mitochondria, 5  $\mu$ g), IMS (intermembrane mitochondrial space, 5  $\mu$ g), MX (mitochondrial matrix, 5  $\mu$ g). Alpha-ketoglutarate dehydrogenase ( $\alpha$ -KDH) is shown as a control of a mitochondrial matrix protein.

Figure S10

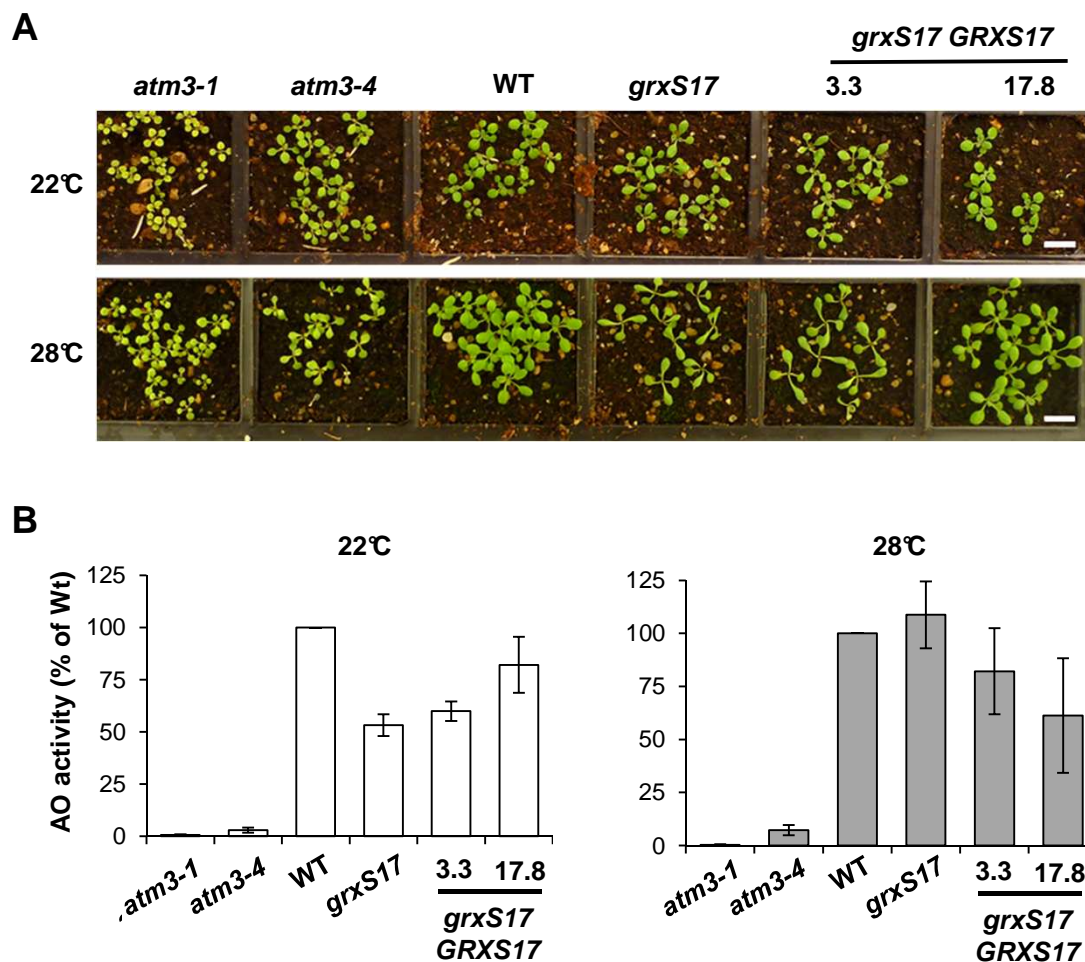


**Figure S10. Growth phenotypes and quantification of aldehyde oxidase enzyme activity in plants modified in *GRXS17* expression.**

*grxS17* knockout seedlings were grown under normal and heat stress conditions and compared to complemented lines (3.3 and 17.8) and wild type (WT). For comparison, a weak (*atm3-4*) and a strong mutant allele (*atm3-1*) of *ATM3* were analysed, which are known to have decreased activities of cytosolic Fe-S enzymes. Plants were grown in long photoperiod (16 h) at 22°C for 14 days (white bars), or shifted to 28°C after 7 days (grey bars). (A) Images of *grxS17* mutants and controls grown under standard conditions and under heat stress. Scale bar = 1 cm. (B) Quantification of the band intensities in native gels (Fig. 7) reflecting the major aldehyde oxidase activity using ImageJ. Activities are shown as percentage of WT levels (mean  $\pm$  SD; n = 3).

Figure S11

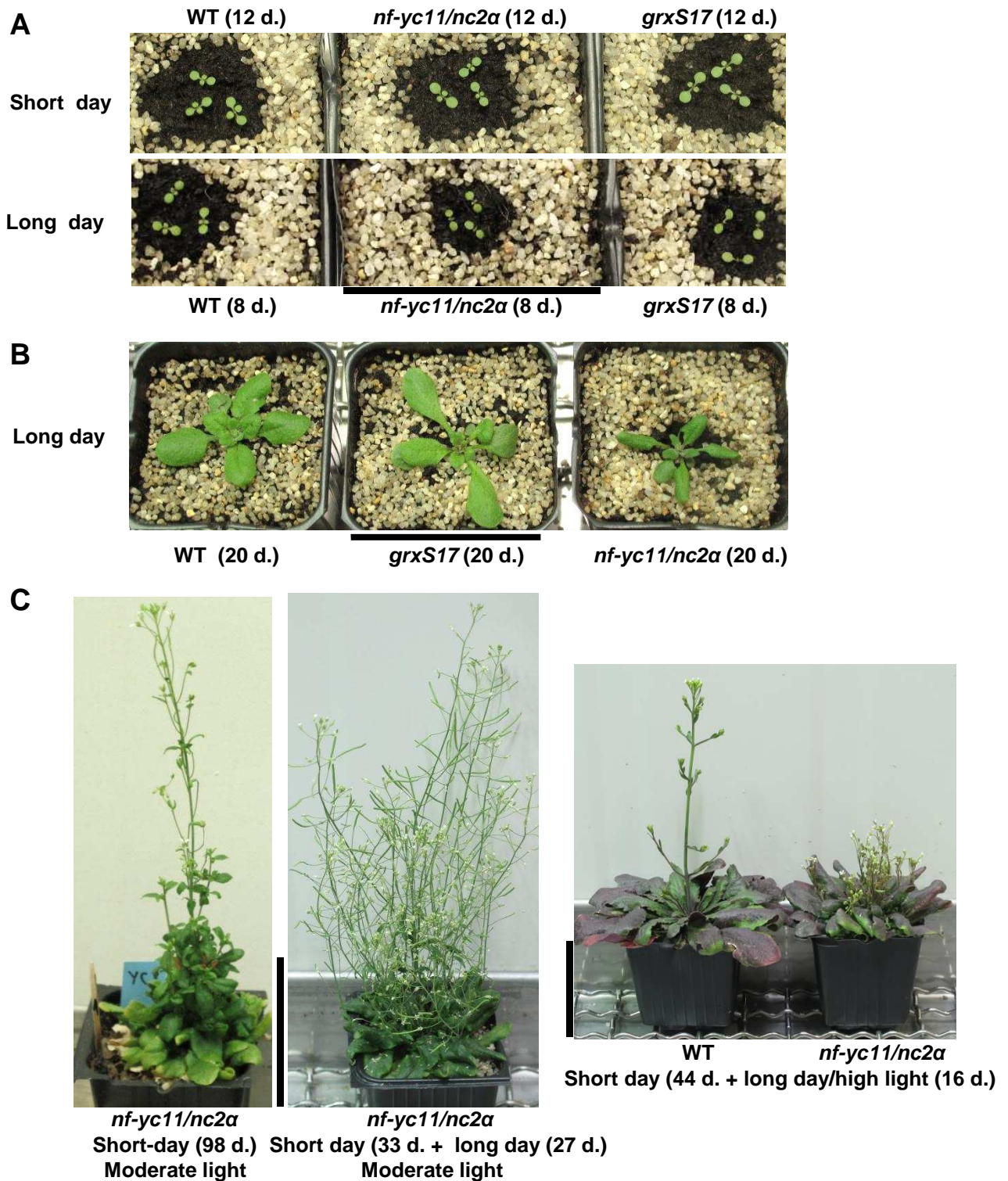


**Figure S11. Development of *nf-yc11/nc2a* plants as a function of light environment**

(A) Development of seedlings in short- and long-day conditions (8-h and 16-h, respectively) at moderate light ( $200 \mu\text{mol photons} \cdot \text{m}^{-2} \cdot \text{s}^{-1}$ ) and  $22^\circ\text{C}$ . (B) Phenotype of plants grown in long-day (16 h photoperiod) and moderate light ( $200 \mu\text{mol photons} \cdot \text{m}^{-2} \cdot \text{s}^{-1}$ ) conditions at  $22^\circ\text{C}$ . (C) Reproductive development of *nf-yc11/nc2a* plants in short- or long-day conditions at moderate or high light ( $200$  or  $500 \mu\text{mol photons} \cdot \text{m}^{-2} \cdot \text{s}^{-1}$ , respectively) and  $22^\circ\text{C}$ . Scale bars: 6 cm. The plant age and culture condition are indicated for each genotype.



**Table SI. Plasmids employed for experiments on yeast.**

<b>Plasmids</b>	<b>Characteristics</b>
pMM993	Sequence coding from amino acid 1-488 of GrxS17 cloned between <i>NotI</i> - <i>PstI</i> sites of pMM221
pMM994	Sequence coding from amino acid 167-252 (M2) of GrxS17 cloned between <i>NotI</i> - <i>PstI</i> sites of pMM221
pMM997	Sequence coding from amino acid 297-383 (M3) of GrxS17 cloned between <i>NotI</i> - <i>PstI</i> sites of pMM221
pMM998	Sequence coding from amino acid 404-488 (M4) of GrxS17 cloned between <i>NotI</i> - <i>PstI</i> sites of pMM221

**Table SII. Yeast strains.**

<b>Strains</b>	<b>Relevant phenotype</b>	<b>Comments</b>
W303-1A	<i>MATa ura3-1 ade2-1 leu2-3,112 trp1-1 his3-11,15</i>	Wild type
W303-1B	As W303-1A but <i>MATα</i>	Wild type
MML100	<i>MATa grx5::kanMX4</i>	Rodríguez-Manzaneque <i>et al.</i> (2002)
MML240	<i>MATa grx5::kanMX4</i> [pMM54( <i>GRX5-3HA</i> )]:: <i>LEU2</i>	Rodríguez-Manzaneque <i>et al.</i> (2002)
MML289	<i>MATα grx5::kanMX4</i>	As MML100, but derived from W303-1B
MML1268	<i>MATa</i> [pMM997( <i>GrxS17-3HA</i> )]:: <i>LEU2</i>	Integration of linear pMM997 in W303-1A
MML1272	<i>MATa</i> [pMM993( <i>GrxS17-3HA</i> )]:: <i>LEU2</i>	Integration of linear pMM993 in W303-1A
MML1274	<i>MATa</i> [pMM994( <i>GrxS17-3HA</i> )]:: <i>LEU2</i>	Integration of linear pMM994 in W303-1A
MML1276	<i>MATa</i> [pMM998( <i>GrxS17-3HA</i> )]:: <i>LEU2</i>	Integration of linear pMM998 in W303-1A
MML1280	<i>MATa grx5::kanMX4</i> [pMM993( <i>GrxS17-3HA</i> )]:: <i>LEU2</i>	Spore from a cross MML 289 x MML1272
MML1282	<i>MATa grx5::kanMX4</i> [pMM994( <i>GrxS17-3HA</i> )]:: <i>LEU2</i>	Spore from a cross MML 289 x MML1274
MML1288	<i>MATa grx5::kanMX4</i> [pMM997( <i>GrxS17-3HA</i> )]:: <i>LEU2</i>	Spore from a cross MML 289 x MML1268
MML1290	<i>MATa grx5::kanMX4</i> [pMM998( <i>GrxS17-3HA</i> )]:: <i>LEU2</i>	Spore from a cross MML 289 x MML1276

**Table SIII. List of primers employed in this study.**

<b>Name</b>	<b>Primers</b>	<b>Characteristics</b>	<b>Organism</b>
MMO 1285	AAACAGCGGCCGCATTATTCATGAAAGGTATTCCT	Upstream oligo for cloning M2 module of <i>AtGRXS17</i> in pMM221. Contains NotI site	Yeast
MMO 1286	AAACACTGCAGAAGATCTTTGAAAGCATCTTT	Downstream oligo for cloning M2 module of <i>AtGRXS17</i> in pMM221. Contains PstI site	Yeast
MMO 1287	AAACAGCGGCCGCCTGTTTCATGAAAGGAAGAC	Upstream oligo for cloning M3 module of <i>AtGRXS17</i> in pMM221. Contains NotI site	Yeast
MMO 1288	AAACACTGCAGCCCTTTCTCGGTCAAGAC	Downstream oligo for cloning M3 module of <i>AtGRXS17</i> in pMM221. Contains PstI site	Yeast
MMO 1289	AAACAGCGGCCGCCTATTCATGAAAGGTTACC	Upstream oligo for cloning M4 module of <i>AtGRXS17</i> in pMM221. Contains NotI site	Yeast
MMO 1290	AAACACTGCAGCTCGGATAGAGTTGCTTTG	Downstream oligo for cloning M4/entire module of <i>AtGRXS17</i> in pMM221. Contains PstI site	Yeast
MMO 1291	AAACAGCGGCCGCAAGCGGTACGGTGAAGGAT	Upstream oligo for cloning the entire <i>AtGRXS17</i> in pMM221. Contains NotI site	Yeast
At4g04950 F	CCCCCATGAGCGGTACGGTGAAGGAT	Forward primer for cloning <i>AtGRXS17</i> and PCR analysis	Arabidopsis
At4g04950 R	CCCCGATCTTACTCGGATAGAGTTGC	Reverse primer for cloning <i>AtGRXS17</i> and PCR analysis	Arabidopsis
At4g04950 Rec-F	GGAATTCCATATGAGCGGTACGGTGAAGG	Forward primer for cloning <i>AtGRXS17</i> in pET-16b expression vector	Arabidopsis
At4g04950 Rec-R	CGGGATCCTTACTCGGATAGAGTTGCTTTG	Reverse primer for cloning <i>AtGRXS17</i> in pET-16b expression vector	Arabidopsis
At4g04950 C33S F	CTTCTGGGCTTCTTGGAGTGATGCTTCGAAGCA	Forward primer for site-directed mutagenesis (Cys-33 to Ser)	Arabidopsis
At4g04950 C33S R	TGCTTCGAAGCATCACTCCAAGAAGCCAGAAG	Reverse primer for site-directed mutagenesis (Cys-33 to Ser)	Arabidopsis
At4g04950 C179S F	CCTGAAGAGCCTAGGAGTGGGTTTAGCAGGA	Forward primer for site-directed mutagenesis (Cys-179 to Ser)	Arabidopsis
At4g04950 C179S R	TCCTGCTAAACCCACTCCTAGGCTCTTCAGG	Reverse primer for site-directed mutagenesis (Cys-179 to Ser)	Arabidopsis
At4g04950 C309S F	GACCAGAAGAACCAAGAGTGGGTTCAAGTGGAAA	Forward primer for site-directed mutagenesis (Cys-309 to Ser)	Arabidopsis
At4g04950 C309S R	TTTCCCACTGAACCCACTCTTTGGTCTTCTGGTC	Reverse primer for site-directed mutagenesis (Cys-309 to Ser)	Arabidopsis
At4g04950 C416S F	GGTTCACCAGATGAACCGAAAAGCGGATTTAGCT	Forward primer for site-directed mutagenesis (Cys-416 to Ser)	Arabidopsis
At4g04950 C416S R	AGCTAAATCCGCTTTTCGGTTCATCTGGTGAACC	Reverse primer for site-directed mutagenesis (Cys-416 to Ser)	Arabidopsis
At5g09810 F	AAAATGGCCGATGGTGAGGATAT	Forward primer for PCR analysis (Actin control)	Arabidopsis
At5g09810 R	CAATACCGTTGTACGACCACT	Reverse primer for PCR analysis (Actin control)	Arabidopsis
At3g12480 F2	TCGACGATTTCTGGATTTGG	Forward primer for PCR and RT-PCR analyses ( <i>AtNF-YC11/NC2α</i> )	Arabidopsis
At3g12480 R2	CCTTCTCTTGAGATGCTGC	Reverse primer for PCR and RT-PCR analyses ( <i>AtNF-YC11/NC2α</i> )	Arabidopsis